Received: 21 February 2020 | Revised: 15 June 2020

DOI: 10.1111/sapm.12328

STUDIES IN APPLIED MATHEMATICS WILEY

ORIGINAL ARTICLE

Stable blow-up dynamics in the L^2-critical and L^2-supercritical generalized Hartree equation

Kai Yang[1] | **Svetlana Roudenko**[1] | **Yanxiang Zhao**[2]

[1] Department of Mathematics & Statistics, Florida International University, Miami, Florida 33199, USA

[2] Department of Mathematics, George Washington University, Washington, District of Columbia

Correspondence
Svetlana Roudenko, Department of Mathematics and Statistics, Florida International University, Miami, FL 33199.
Email: sroudenko@fiu.edu

Funding information
Simons Foundation, Grant/Award Number: 357963; National Science Foundation, DMS, Grant/Award Numbers: 1151618/1929029, 1815873/1927258

Abstract

We study stable blow-up dynamics in the generalized Hartree equation with radial symmetry, which is a Schrödinger-type equation with a nonlocal, convolution-type nonlinearity:

$$iu_t + \Delta u + \left(|x|^{-(d-2)} * |u|^p\right)|u|^{p-2}u = 0,$$
$$x \in \mathbb{R}^d.$$

First, we consider the L^2-critical case in dimensions $d = 3, 4, 5, 6, 7$ and obtain that a generic blow-up has a self-similar structure and exhibits not only the square root blowup rate $\|\nabla u(t)\|_{L^2} \sim (T-t)^{-\frac{1}{2}}$, but also the *log-log* correction (via asymptotic analysis and functional fitting), thus, behaving similarly to the stable blow-up regime in the L^2-critical nonlinear Schrödinger equation. In this setting, we also study blow-up profiles and show that generic blow-up solutions converge to the rescaled Q, a ground state solution of the elliptic equation $-\Delta Q + Q - (|x|^{-(d-2)} * |Q|^p)|Q|^{p-2}Q = 0$.

We also consider the L^2-supercritical case in dimensions $d = 3, 4$. We derive the profile equation for the self-similar blow-up and establish the existence and local uniqueness of its solutions. As in the NLS L^2-supercritical regime, the profile equation exhibits branches of nonoscillating, polynomially decaying (multi-bump) solutions. A numerical scheme of putting

constraints into solving the corresponding ordinary differential equation is applied during the process of finding the multi-bump solutions. Direct numerical simulation of solutions to the generalized Hartree equation by the dynamic rescaling method indicates that the $Q_{1,0}$ is the profile for the stable blow-up. In this supercritical case, we obtain the blow-up rate without any correction. This blow-up happens at the focusing level 10^{-5}, and thus, numerically observable (unlike the L^2-critical case). In summary, we find that the results are similar to the behavior of stable self-similar blowup solutions in the corresponding settings for the nonlinear Schrödinger equation. Consequently, one may expect that the form of the nonlinearity in the Schrödinger-type equations is not essential in the stable formation of singularities.

KEYWORDS
adiabatic regime, Choquard equation, convolution nonlinearity, dynamic rescaling, Hartree equation, log-log blow-up, multi-bump profile, nonlocal potential

1 | INTRODUCTION

We consider the Cauchy problem of the generalized Hartree (gHartree) equation:

$$\begin{cases} iu_t + \Delta u + \left(\frac{1}{|x|^b} * |u|^p\right)|u|^{p-2}u = 0, \quad (t,x) \in \mathbb{R} \times \mathbb{R}^d, \\ u_0 = u(x,0) \in H^1(\mathbb{R}^d). \end{cases} \tag{1}$$

Here, the $*$ represents the convolution in $\mathbb{R}^d$ with the convolution power $0 < b < d$ and the nonlinearity power typically $p \geq 2$, though we will also consider cases with $p > 1$ (details below). When $p = 2$, Equation (1) is the well-known Hartree equation

$$iu_t + \Delta u + \left(\frac{1}{|x|^b} * |u|^2\right)u = 0, \tag{2}$$

which arises, for example, in the description of dynamics in Bose-Einstein condensates (BEC) with long-range attractive interaction, proportional to $1/|x|^b$ and arbitrary angular dependence, for example, see Refs. 1–3. It appears as the mean field limit of quantum Bose gases,[4] and is also used to describe a certain type of a trapped electron,[5] see also Refs. 6–9. Within the pseudo-relativistic

setting, if the Laplacian in (1) is replaced by $\sqrt{m^2-\Delta}$ and $b=1$, then the equation

$$iu_t+\sqrt{m^2-\Delta}\,u+\left(\frac{1}{|x|}*|u|^2\right)u=0,\quad x\in\mathbb{R}^3, \tag{3}$$

appears in the description of boson stars, see Ref. 10.

The well-posedness theory of Equation (2) is obtained by Ginibre and Velo in Ref. 6 (see also Ref. 11). For a general nonlinearity $p\geq 2$, the H^1 well-posedness is obtained in Ref. 12. (It is also possible to consider H^s well-posedness[1] for $0\leq s<1$, and in certain cases for $s>1$, for exact statements, see Refs. 12, 13 and a review with alternative proofs.[14]) Let (T_-,T_+) denote the maximal time interval of existence of solutions to (1), that is, for given initial data $u_0\in H^1(\mathbb{R}^d)$, one has $u(t)\in C((T_-,T_+),H^1(\mathbb{R}^d))$. Without loss of generality, we consider the solutions in forward time $T>0$. We say that the solution to Equation (1) is locally well-posed if $T<\infty$, and it is globally well-posed if $T=\infty$. If $T<\infty$, then we say that the solution blows up in finite time.

During their lifespans, solutions of (1) conserve mass and energy (Hamiltonian):

$$M[u(t)]:=\int_{\mathbb{R}^d}|u(x,t)|^2dx=M[u_0], \tag{Mass}$$

$$E[u(t)]:=\frac{1}{2}\int_{\mathbb{R}^d}|\nabla u|^2dx-\frac{1}{2p}\int_{\mathbb{R}^d}\left(\frac{1}{|x|^b}*|u|^p\right)|u|^pdx=E[u_0]. \tag{Energy}$$

Since we only consider radial solutions, we omit conservation of momentum.

Equation (1) has scaling invariance similar to the nonlinear Schrödinger (NLS) equation. Let $u(x,t)$ be the solution to (1), then one can see that $u_\lambda(x,t)=\lambda^{\frac{d-b+2}{2(p-1)}}u(\lambda x,\lambda^2 t)$ is also a solution to (1).

The criticality comes from the scaling invariance of $\dot{H}^s$ norm, that is, $\|u(x,t)\|_{\dot{H}^s_x}=\|u_\lambda(x,t)\|_{\dot{H}^s_x}$. The direct calculation leads us to

$$s=\frac{d}{2}-\frac{d-b+2}{2(p-1)}. \tag{4}$$

If $s=0$, Equation (1) is referred to as the L^2-critical (or mass-critical as it preserves the mass, L^2-norm). If $s=1$, the equation is $\dot{H}^1$-critical (or energy-critical as it preserves the energy). If $0<s<1$, the equation is mass-supercritical and energy-subcritical (or inter-critical), and finally, it is energy-supercritical if $s>1$.

When $s\geq 0$, solutions can blow-up in finite time, for example, initial data with negative energy and finite initial variance $\mathcal{V}(0)<\infty$, where $\mathcal{V}(t)=\int_{\mathbb{R}^d}|x|^2|u(x,t)|^2dx$, by a standard convexity or virial argument (as in the NLS equation), see also Refs. 1,2, or can exist globally in time (global well-posedness holds on some sets of solutions, see Refs. 6, 11–13). If the solution blows up in finite time in the energy-subcritical case, it means that $\lim_{t\nearrow T}\|\nabla u(\cdot,t)\|_{L^2}=\infty$. It is more delicate to track the blow-up in the energy-critical case as well as in the supercritical, which we discuss later.

In this paper, we restrict our attention to the power $b=d-2$ and the dimensions $d>2$. There are two reasons for that. The first one is that this is exactly the case when the convolution is the

[1] Or even homogeneous Sobolev space $\dot{H}^s$ wellposedness.

fundamental solutions of the Poisson equation, and thus, the nonlocal term can be written as

$$\frac{1}{|x|^{d-2}} * |u|^p = \alpha(d)(-\Delta)^{-1}|u|^p,$$

where $\alpha(d)$ is the dimensional constant. In this case, the scaling critical index (4) becomes

$$s_c = \frac{d}{2} - \frac{2}{p-1}. \tag{5}$$

The dimensional constant $\alpha(d)$ can be removed by scaling, thus, Equation (1) is reduced to

$$\begin{cases} iu_t + \Delta u + \left((-\Delta)^{-1}|u|^p\right)|u|^{p-2}u = 0, \ (t,x) \in [0,T) \times \mathbb{R}^d, \\ u_0 = u(x,0) \in H^1(\mathbb{R}^d). \end{cases} \tag{6}$$

The second reason for choosing $b = d-2$, is the solitary wave solutions to (6). Similar to the NLS equation, when $b = d-2$ and $p < 1 + \frac{4}{d-2}$ $(s < 1)$, we consider standing wave solutions to (6) of the form $u(x,t) = e^{it}Q(x)$ with Q being the positive and vanishing at infinity solution of

$$-\Delta Q + Q - \left(\frac{1}{|x|^{d-2}} * |Q|^p\right)|Q|^{p-2}Q = 0, \tag{7}$$

or equivalently,

$$-\Delta Q + Q - \left((-\Delta)^{-1}|Q|^p\right)|Q|^{p-2}Q = 0. \tag{8}$$

The existence and uniqueness of the real, positive, vanishing at infinity solution to (7), or (8), are obtained for $p = 2$ in Ref. 5 $(d = 3)$, Ref. 15 $(d = 4)$, Ref. 12 $(2 < d < 6)$; for $p = 2 + \epsilon$ in Ref. 16, otherwise, it is not known; the existence with decay and other properties in a general case is investigated in Ref. 17; see also an excellent review in Ref. 18.

This solution is known as the ground state solution, which we also denote by Q. Note that the ground state solution is radially symmetric $Q = Q(r)$ and is exponentially decaying at infinity for $p \geq 2$, see, for example, Ref. 17. Although there is no explicit formula for the ground state solution Q, we can obtain the profiles numerically (e.g., via the renormalization method similar to the NLS in (Ref. 19, chapter 28), see the Appendix).

In this paper, we are interested in studying stable blow-up dynamics of solutions to Equation (6) in the L^2-critical case $(p = 1 + \frac{4}{d})$ and in the L^2-supercritical case $(p > 1 + \frac{4}{d})$. As in the NLS equation, in the L^2-critical case, some blow-up solutions (of minimal mass) can be obtained via the pseudo-conformal transformation. However, these blow-up solutions are unstable. We are interested in stable blow-up solutions of (6), at least in those solutions, which can be observed numerically from a generic initial data (such as Gaussian initial conditions). The scaling invariance is the underlying mechanism for the dynamic rescaling method that we use to simulate the blow-up solutions (this is in the spirit of Refs. 20, 21, also Refs. 22, 23, see Section 3 for details). In particular, we will investigate the blow-up rate and blow-up profiles of singular solutions to the gHartree equation (6) in the critical and supercritical settings.

We first recall the definition of the blow-up rate (e.g., from Refs. 24, 25, or 19), which is used in the standard NLS equation.

Definition 1. The blow-up rate is the function $f(t)$ (e.g., $f(t) = (T-t)^{-\frac{1}{2}}$) such that

$$\lim_{t \nearrow T} \frac{\|\nabla u(t)\|_{L_x^2}}{f(t)} = C, \tag{9}$$

where C is a constant.

The above definition uses the $\dot{H}^1$ norm, note that due to scaling invariance when $s_c = 1$, the norm $\|u(t)\|_{\dot{H}^1}$ becomes constant, and when $s_c > 1$, then $\|u(t)\|_{\dot{H}^1}$ decreases to zero (see (35) with $L(t) \to 0$). On the other hand, in the numerical simulations we observe that the solution is concentrating at a point with its amplitude growing to infinity in finite time. Thus, instead of tracking the $\dot{H}^1$ norm, one can also study the blow-up rate in terms of the L^∞ norm.

Definition 2. The blow-up rate[2] is the function $f(t)$ (e.g., $f(t) = (T-t)^{-\frac{1}{2}}$) such that

$$\lim_{t \nearrow T} \frac{\|u(t)\|_{L_x^\infty}}{f(t)} = C, \tag{10}$$

where C is a constant.

For the L^2-critical NLS equation, it is known that Definitions 1 and 2 are equivalent, see Refs. 11 and 26. The study of blow-up rates go back to the 1970s, mainly in the two-dimensional cubic NLS (L^2-critical) and, in part, for the 3D cubic NLS (L^2-supercritical) equations, see Refs. 27–29. From scaling and local well-posedness, it follows that the lower bound on the blow-up rate is $(T-t)^{-\frac{1}{2}}$. In 1986, McLaughlin et al. in Ref. 30, introduced the dynamic rescaling method to track the blow-up profile and the rate, and suggested that there should be a correction terms to the rate $(T-t)^{-\frac{1}{2}}$. Previously, Talanov (1978), Wood (1984) and Rypdal and Rasmussen (1986) suggested the rate $(|\ln(T-t)|/(T-t))^{\frac{1}{2}}$ from a different approach (see Refs. 31–33). Using the far asymptotics of the ground state, and considering a slightly supercritical equation by treating the dimension d as a continuous parameter, Landman et al. in Ref. 20, and also LeMesurier et al. in Ref. 50, (see also an earlier work of Fraiman[34]) concluded that the rate of the stable blow-up is of the form $(\ln|\ln(T-t)|/(T-t))^{\frac{1}{2}}$, now commonly referred to as the *log-log* law, see also Ref. 35–37 and books.[19,21] We note that numerically it is not possible (at least with the current computational power) to observe such a double log correction, however, the asymptotic analysis (e.g., as in Ref. 21) produces such a correction; numerically, it is only possible to do the functional fitting and examine stabilization properties of the convergence (see Refs. 22, 38, also Subsection 4.2; see also Refs. 39, 40). This *log-log* rate holds extremely close to the blow-up time, and before the singularity formation gets into the *log-log* regime, it goes through the adiabatic phase, which has been described by Malkin or Fibich adiabatic laws (see Refs. 41, 42); the rate in that penultimate regime is proportional to $(|\ln(T-t)|^\gamma/(T-t))^{\frac{1}{2}}$, see Ref. 38, for the 2D cubic NLS or our work[22] for various other dimensions in the L^2-critical setting.

[2] For solutions concentrating at a point.

Theoretical studies of stable self-similar blow-up dynamics, including rates, in the L^2-critical NLS-type equations have been going on since the 2000s (starting with Galina Perelman's work for the 1D quintic NLS[43], followed by a series of works by Merle and Raphael[44,45]). Various perturbations of nonlinearity have been studied as well, tracking the blow-up rates for various singular solutions, for example, see Refs. 46 and 47, though most of these works do not get stable blow-up solutions (breaking radial symmetry or other perturbations will break the initial geometry or set-up and will force the solution to blow-up in the *log-log* regime, provided enough mass is available). Although various perturbations of nonlinearities have been considered in the literature (for example, in the L^2-critical setting), it is far from being understood how blow-up dynamics depends on the *form* of the nonlinearity (e.g., if the nonlinearity has a significant influence on the stable blow-up rate). This work is a step in that direction. We study how a *nonlocal* nonlinear term affects the stable blow-up dynamics. This is also important in connection with understanding gravitational collapse of (3), where currently only the existence of blow-up is known, see Ref. 4 and also Ref. 15.

In this paper, we investigate the following conjectures:

Conjecture 1 (L^2-critical gHartree)**.** *A stable blow-up solution to the L^2-critical gHartree equation has a self-similar structure and comes with the rate*

$$\lim_{t\to T}\|\nabla u(\cdot,t)\|_{L^2_x}=\left(\frac{\ln|\ln(T-t)|}{2\pi(T-t)}\right)^{\frac{1}{2}}\quad as\quad t\to T,$$

known as the log-log *rate. The solution blows up in a self-similar regime with profile converging to a rescaled profile Q, which is a ground state solution of (7), namely,*

$$u(x,t)\sim\frac{1}{L(t)^{\frac{d}{2}}}Q\left(\frac{x-x(t)}{L(t)}\right)e^{i\gamma(t)}$$

with time-dependent parameters $L(t)$, $x(t)$, and $\gamma(t)$, converging when $t\to T$ as follows: $x(t)\to x_c$ (the blow-up center), $\gamma(t)\to\gamma_0$ (for some $\gamma_0\in\mathbb{R}$) and $L(t)\sim(\frac{2\pi(T-t)}{\ln|\ln(T-t)|})^{\frac{1}{2}}$.

The stable blow-up dynamics in the L^2-critical gHartree equation is similar to the stable blow-up dynamics in the L^2-critical NLS equation.

Conjecture 2 (L^2-supercritical gHartree)**.** *A stable blow-up solution for the L^2-supercritical gHartree equation is of the self-similar form*

$$u(x,t)\sim\frac{1}{L(t)^{\frac{2}{p-1}}}Q\left(\frac{x-x(t)}{L(t)}\right)\exp\left(i\theta+\frac{i}{2a}\log\frac{T}{T-t}\right)\quad as\quad t\to T,\tag{11}$$

where the blow-up profile Q is the $Q_{1,0}$ solution of the profile equation (16) with the specific constant a, the rate $L(t)=(2a(T-t))^{1/2}$, and $x(t)\to x_c$, the blow-up center (see Subsection 2.1 for the notation and details). Consequently,

$$\|\nabla u(\cdot,t)\|_{L^2_x}\sim\frac{1}{L(t)^{1-s_c}}=(2a(T-t))^{-\frac{1}{2}(1-s_c)}\quad as\quad t\to T.$$

This dynamics is similar to the stable blow-up dynamics in the L^2-supercritical NLS equation.

We prove existence of profiles Q to (16) and find their decay before we numerically investigate the above Conjectures. We give numerical confirmation to Conjecture 1 in dimensions $d = 3, 4, 5, 6, 7$ and to Conjecture 2 in dimensions $d = 3, 4$. In particular, we show that the rates in the stable blow-up dynamics do not depend on the local or nonlocal type of nonlinearity in the NLS-type equation, at least in the radial case. The profile in the L^2-critical case is a ground state solution of (8) and in the L^2-supercritical regime, the profile equation (16) exhibits branches of slowly oscillating multi-bump solutions.

To study the blow-up solutions, we adapt the dynamic rescaling method to the generalized Hartree equation and use it in both critical and supercritical cases. For the L^2-critical case, we find that generic blow-up happens with the rate $(\ln|\ln(T-t)|/(T-t))^{\frac{1}{2}}$, which we also refer to as the *log-log* blow-up rate, with the self-similar blow-up profiles converging to Q up to rescaling, that is, $|u(x,t)| \sim |L^{-\frac{d}{2}}(t)Q(x/L(t))|$, where $L(t) \approx (\ln|\ln(T-t)|/(T-t))^{\frac{1}{2}}$. For the L^2-supercritical case, we obtain that the blow-up rate is $\|\nabla u(t)\|_{L^2_x} \sim (T-t)^{-\frac{1}{2}(1-s_c)}$, and we observe that it also blows up with the self-similar profile Q, which is different from a ground state solution of (7). We show the existence and the "local uniqueness" of such self-similar profile Q for the case $0 < s_c < 2$. Numerically, we find that such Q can have multiple slowly decaying solutions. Similar to the NLS L^2-supercritical case Ref. 21, the existence of complex solutions of the rescaled static states Q and the slow decay (not in L^2) makes it challenging to analyze the supercritical blow-up dynamics. Nevertheless, we do find the blow-up profile and the blow-up rate in this case, see Section 5.

This paper is organized as follows. In Section 2, we discuss existence and decay of profiles. In Section 3, we describe the dynamic rescaling method for the gHartree equation. In Section 4, we discuss the L^2-critical case, obtaining the square root blow-up rate with the *log-log* correction. Besides numerical and asymptotic investigations, we also discuss the adiabatic regime occurring prior to the *log-log* regime. We also observe that blow-up profiles converge to the rescaled ground state Q in our numerical simulations. In Section 5, we discuss the L^2-supercritical cases (including $s_c > 1$). Numerically, we obtain the profile $Q_{1,0}$, and justify that the blow-up solutions do converge to that blow-up profiles. We also obtain the blow-up rates, with the precision of 10^{-5} to the predicted blow-up rates. We finish with the Appendix discussing the computation of Q via the renormalization method.

Notation. We consider the homogeneous $\dot{H}^s$ and inhomogeneous H^s Sobolev spaces defined as follows: the space $\dot{H}^s$ is equipped with the norm $\|u\|_{\dot{H}^s(\mathbb{R}^d)} = \|D^s u\|_{L^2(\mathbb{R}^d)}$, where the operator D^s, the Riesz potential, is defined as $\widehat{D^s f}(\xi) = |\xi|^s \hat{f}(\xi)$; the inhomogeneous H^s Sobolev space is equipped with the norm $\|u\|_{H^s(\mathbb{R}^d)} = \|J^s u\|_{L^2(\mathbb{R}^d)}$, where the operator J^s, the Bessel potential of order s, is defined as $\widehat{J^s f}(\xi) = (1+|\xi|^2)^{\frac{s}{2}} \hat{f}(\xi)$.

2 | PRELIMINARIES ON GROUND STATES AND PROFILES

We start with applying the scaling invariance property to finite time existing solutions of (6), which makes solutions of the rescaled equation exist globally in time. For consistency with literature, we

write the power $p = 2\sigma + 1$ and set (here, $r = |x|$)

$$u(r,t) = \frac{1}{L^{1/\sigma}(t)} v(\xi,\tau), \qquad \xi = \frac{r}{L(t)}, \quad \text{and} \quad \tau = \int_0^t \frac{ds}{L^2(s)}. \tag{12}$$

The direct calculation of this substitution into (6) yields

$$iv_\tau + ia(\tau)\Big(\frac{v}{\sigma} + \xi v_\xi\Big) + \Delta v + \big((-\Delta)^{-1}|v|^{2\sigma+1}\big)|v|^{2\sigma-1}v = 0, \tag{13}$$

where

$$a(\tau) = -L\frac{dL}{dt} = -\frac{d\ln L}{d\tau}. \tag{14}$$

As in the NLS case, studying the parameter $L(t)$ will clarify the blow-up rate of the solutions, which differs for the L^2-critical versus the L^2-supercritical cases, exactly because of the asymptotic behavior of the parameter $a(\tau)$ (we show that in the gHartree equation it will tend to zero in the L^2-critical case and to a nonzero constant in the supercritical case). Therefore, we study those cases separately.

Before that, we discuss some preliminaries on the profile equation and suitable solutions for the blow-up profiles. For that we assume that $a(\tau) \to a$, some specific constant, which we will obtain later numerically.

We note that the behavior of solutions as $t \to T$ in the original equation (6) can be reconstructed from those to the rescaled equation (13) as $\tau \to \infty$.

2.1 | Profile equation

We separate variables $v(\xi,\tau) = e^{i\tau}Q(\xi)$ in (13) and obtain

$$\Delta_\xi Q - Q + ia(\tau)\left(\frac{Q}{\sigma} + \xi Q_\xi\right) + ((-\Delta)^{-1}|Q|^{2\sigma+1})|Q|^{2\sigma-1}Q = 0, \tag{15}$$

here, $\Delta_\xi := \partial_{\xi\xi} + \frac{d-1}{\xi}\partial_\xi$ denotes the Laplacian with radial symmetry. Assuming that $a(\tau)$ converges to a constant a, instead of (15) in this section we study the following problem

$$\begin{cases} \Delta_\xi Q - Q + ia\left(\frac{Q}{\sigma} + \xi Q_\xi\right) + ((-\Delta)^{-1}|Q|^{2\sigma+1})|Q|^{2\sigma-1}Q = 0, \\ Q_\xi(0) = 0, \qquad Q(0) \in \mathbb{R}, \qquad Q(\infty) = 0. \end{cases} \tag{16}$$

The first condition for Q indicates that the local maximum is at zero. The second condition on Q shows that we fix the phase of the solutions, since the equation is phase invariant; the last condition means that $Q(\xi) \to 0$ as $\xi \to \infty$. Moreover, we will seek for solutions, which have $|Q(\xi)|$ decreasing monotonically with ξ, without oscillations as $\xi \to \infty$.

Understanding solutions of the stationary equation in (16) leads to a set of possible profiles, one of which corresponds to the profile of stable blow-up. For the L^2-critical case, this equation is simplified (due to a being zero), however, we still ought to investigate the L^2-supercritical case

(with nonzero a but asymptotically approaching zero), since the correction in the blow-up rate comes exactly from that. We refer to the above equation as the *profile equation* and discuss the existence and local uniqueness theory of its solutions.

2.2 | Existence theory for profile solutions

Several properties of solutions to (16) are established in the following lemmas. We mention that while the statements are similar to the ones in the NLS case (see Ref. 23), the calculations differ and often have extra terms and assumptions, compared to the pure power case.

Lemma 1. *Let $s_c = \frac{d}{2} - \frac{1}{\sigma}$. Assume $d > 2$ and $\sigma \geq \frac{1}{2}$. If $Q(\xi)$ is the solution of Equation (16), then*

$$\frac{\xi^{d-2}}{2}\left|\xi Q_\xi + \frac{Q}{\sigma}\right|^2 + \frac{\xi^d}{2}|Q|^2\left(\left(\frac{1}{2\sigma+1}(-\Delta)^{-1}|Q|^{2\sigma+1}\right)|Q|^{2\sigma-1} - \frac{1}{\sigma^2\xi^2}\right) + \frac{2-s_c}{2\sigma+1}\int_0^\xi V(Q)\, s^{d-1}\, ds = (1-s_c)\int_0^\xi |Q_\xi|^2 s^{d-1}\, ds, \tag{17}$$

and

$$2\,\mathrm{Im}(\xi Q_\xi \bar{Q}) + 2(d-2)\,\mathrm{Im}\int_0^\xi Q_\xi \bar{Q}\, ds + 2a\left(\frac{1}{\sigma} - 1\right)\int_0^\xi |Q|^2 s\, ds + a|\xi|^2|Q|^2 = 0, \tag{18}$$

where

$$V(Q) \overset{\text{def}}{=} ((-\Delta)^{-1}|Q|^{2\sigma+1})|Q|^{2\sigma+1}. \tag{19}$$

Proof. Multiply (16) by $\Delta\bar{Q}\xi^{d-1}$, take the imaginary part and integrate from 0 to ξ. This gives

$$a\,\mathrm{Re}\int_0^\xi \left(\xi Q_\xi + \frac{Q}{\sigma}\right)\Delta\bar{Q}\xi^{d-1} + \mathrm{Im}\int_0^\xi ((-\Delta)^{-1}|Q|^{2\sigma+1})|Q|^{2\sigma-1}Q\Delta\bar{Q}\xi^{d-1} = 0. \tag{20}$$

The first part is equivalent to

$$a\left(\xi^{d-2}\,\mathrm{Re}\left(\xi\bar{Q}_\xi\frac{Q}{\sigma}\right) + \frac{\xi^d}{2}|Q_\xi|^2 + \left(\frac{d}{2} - \frac{1}{\sigma} - 1\right)\int_0^\xi |Q_\xi|^2\, s^{d-1}\, ds\right), \tag{21}$$

and, by using (16) to express $\Delta\bar{Q}$, the second part of (20) yields

$$a\left(\frac{\xi^d}{2(2\sigma+1)}V(Q) - \frac{1}{2\sigma+1}\left(\frac{d}{2} - \frac{1}{\sigma} - 2\right)\int_0^\xi V(Q)\, s^{d-1}\, ds\right). \tag{22}$$

Putting together these two parts gives the identity (17).

The second identity (18) is obtained by multiplying $2\xi\bar{Q}$, integrating from 0 to ξ, and then taking the imaginary part. ∎

Lemma 2. *Suppose $Q(\xi)$ is the $C^2[0,\infty)$ solution of Equation (16) for $d > 2$ and $\sigma \geq \frac{1}{2}$. If[3] $0 < s_c \leq 2$, then $|Q(\xi)|$ and $|Q_\xi(\xi)|$ are bounded.*

Proof. Since Equation (16) has two derivatives, both $Q(\xi)$ and $Q_\xi(\xi)$ are continuous. Thus, both $Q(\xi)$ and $Q_\xi(\xi)$ are bounded in the interval $\xi \in [0, M]$ for any $M > 0$. Thus, it suffices to consider the case when $\xi \to \infty$ (we follow the argument in Ref. 48 and Ref. 23 for the NLS).

For that, from (17), we claim that if $|Q_\xi|$ is bounded, so is $|Q|$. To the contrary, suppose that $|Q_\xi|$ is bounded but $|Q|$ is not as $\xi \to \infty$. We consider two cases: $s_c \geq 1$ and $s_c < 1$.

For $s_c \geq 1$, the right-hand side (RHS) of (17) is not positive, while the left-hand side (LHS) of (17) is strictly positive for sufficiently large ξ. We reach a contradiction immediately.

If $s_c < 1$, then by dropping the first and third terms (which are positive) in (17), for sufficiently large ξ, we have

$$0 \leq c\,\frac{\xi^d}{2}|Q|^2 \leq \frac{\xi^d}{2}|Q|^2\left(\frac{1}{2\sigma+1}((-\Delta)^{-1}|Q|^{2\sigma+1})|Q|^{2\sigma-1} - \frac{1}{\sigma^2\xi^2}\right)$$
$$\leq \text{LHS of (17)} = \text{RHS of (17)} \leq (1-s_c)\,\xi^d. \tag{23}$$

Comparing the growth for large ξ on both sides of the above inequality, yields boundedness of $|Q|$.

We next show that $|Q_\xi|$ is bounded as $\xi \to \infty$. We prove the boundedness of $|Q_\xi|$ by contradiction. Suppose $|Q_\xi|$ is not bounded, that is, $\limsup_{\xi\to\infty} Q_\xi(\xi) = \infty$. Then, there exists a monotonic increasing sequence $\{\xi_j\}_{j=0}^{\infty}$ such that $|Q_\xi(\xi_j)| \to \infty$ as $j \to \infty$ (or equivalently, as $\xi_j \to \infty$). Since $\xi_j \to \infty$, for any $M > 0$, there exists an index j such that $\xi_j > M$.

We again consider cases $s_c \geq 1$ and $s_c < 1$ separately. When $s_c \geq 1$, the RHS of (17) is nonpositive, while the LHS of (17) will be strictly positive for ξ_j with j sufficiently large, leading to a contradiction.

By a direct calculation, we rewrite (17) for $0 < \delta < 1$ as

$$(1-\delta)|Q_\xi|^2 + \delta\left|Q_\xi + \frac{Q}{\delta\sigma\xi}\right|^2 + \frac{1}{2\sigma+1}V(Q) - \frac{|Q|^2}{\delta\sigma^2\xi^2} + \frac{(2-s_c)}{(2\sigma+1)}\frac{2}{\xi^d}\int_0^\xi V(Q)\,s^{d-1}ds$$
$$= \frac{2(1-s_c)}{\xi^d}\int_0^\xi |Q_\xi|^2\,s^{d-1}\,ds. \tag{24}$$

If $s_c < 1$, then the term $\frac{(2-s_c)}{(2\sigma+1)}\frac{2}{\xi^d}\int_0^\xi V(Q)s^{d-1}ds > 0$. Also, for any fixed $0 < \delta < 1$, there exists an $M > 0$ such that for any $\xi_j > M$, the difference of the third and fourth terms is positive

$$\frac{1}{2\sigma+1}V(Q) - \frac{|Q|^2}{\delta\sigma^2\xi_j^2} = |Q|^2\left(\left(\frac{1}{2\sigma+1}(-\Delta)^{-1}|Q|^{2\sigma+1}\right)|Q|^{2\sigma-1} - \frac{1}{\delta\sigma^2\xi_j^2}\right) > 0.$$

[3] The reason for the restriction $s_c < 2$ is to keep the third term in (17) positive.

For the same ξ_j, we bound the RHS of (24) as

$$\frac{2(1-s_c)}{\xi_j^d}\int_0^{\xi_j}|Q_\xi|^2\xi^{d-1}d\xi \le \frac{2(1-s_c)}{d}|Q_\xi(\xi_j)|^2.$$

Thus, collecting the above observations into (24), and using that $d>2$ (thus, $\frac{2}{d}<1$), we get

$$(1-\delta)\frac{2}{d}|Q_\xi(\xi_j)|^2 \le \text{ LHS of (24)} \le \frac{2(1-s_c)}{d}|Q_\xi(\xi_j)|^2. \tag{25}$$

Taking $0<\delta<s_c<1$, we reach the contradiction for any $\xi_j>M$. We can now conclude that both $|Q_\xi|$ and $|Q|$ are bounded. ■

We next discuss the existence theory for (16).

Theorem 1 (Existence of Q). *Define $s_c=\frac{d}{2}-\frac{1}{\sigma}$. If $0<s_c\le 2$, $d>2$ and $\sigma\ge\frac{1}{2}$, for any given initial value $Q(0)\in\mathbb{R}$ and constant $a>0$, Equation (16) has a unique solution in $C^2[0,\infty)$.*

Proof. The problem is equivalent to the Volterra integral equation:

$$\begin{aligned}Q(\xi) &= Q(0)-ia\int_0^\xi sQ(s)ds+\frac{1}{d-2}\\ &\times\int_0^\xi\left[1+ia\left(d-\frac{1}{\sigma}\right)-((-\Delta)^{-1}|Q(s)|^{2\sigma+1})|Q(s)|^{2\sigma-1}\right]Q(s)\left(s-\frac{s^{d-1}}{\xi^{d-2}}\right)ds,\quad Q(\infty)=0.\end{aligned} \tag{26}$$

Equation (26) is of the form

$$Q(\xi)=Q(0)+\int_0^\xi g(s,\xi,Q(s))ds,\quad Q(\infty)=0. \tag{27}$$

From the theory of Volterra integral equation (see exact statements in Ref. 23, as well as the application in the NLS case, which is following (Ref.[49], Theorem 3.2.2)), Equation (27) has a unique solution on the interval $\xi\in[0,M]$ for some fixed $M>0$, since $g(s,\xi,Q(s))$ is continuous. This result can be extended to $M=\infty$, since $|Q(\xi)|$ is bounded (see Ref. 23, Theorem 2.1 and Ref. 49, Theorem 3.3.6)). From Lemma 2, it follows that the integral equation (26) has a unique solution. We next note that Q is the solution not only to Equation (26) or (27), but also to the differential equation (16), and thus, differentiating Q twice classically, it gives $Q\in\mathbb{C}^2[0,\infty)$, finishing the proof. ■

Remark 1. If $s_c=0$ (thus, $a=0$), the equation in (26) reduces to

$$Q(\xi)=Q(0)+\frac{1}{d-2}\int_0^\xi\left[1-((-\Delta)^{-1}|Q(s)|^{2\sigma+1})|Q(s)|^{2\sigma-1}\right]Q(s)\left(s-\frac{s^{d-1}}{\xi^{d-2}}\right)ds,$$

and given the initial value of $Q(0)$, the uniqueness holds from a similar argument due to Volterra integral theory. The values of $Q(0)$ are unknown a priori in the L^2-critical case, nevertheless, our numerical solver converges to the same Q regardless of initial condition, see the Appendix.

Corollary 1. *For $d > 2$ and $s_c > 0$, if $\sigma = 1$, then $|Q(\xi)| \lesssim \xi^{-1}$ for ξ large enough (recall that ξ is radial variable here, and thus, nonnegative).*

Proof. When $\sigma = 1$, the term $2a(\frac{1}{\sigma} - 1)\int_0^\xi s|Q|^2 ds$ in (18) cancels. Then, the rest of the proof is the same as in Ref. 48, (Theorem 2.2) and Ref. 23, (Corollary 2.7). ∎

Remark 2. For other values of σ, one would obtain the decay of Q as $|\xi|^{-1/\sigma}$, which can be proved in various ways: as in the NLS (see Ref. 23, Theorem 2.2), or by examining the asymptotic (large distance) behavior as in (Ref. 50, section 3.1), which we will do in the next subsection.

Remark 3. The reason for the lower bound $s_c > 0$ is indeed necessary, since Equation (16) does not have "admissible" solutions as we prove below in Proposition 3.

2.3 | Asymptotic behavior of the L^2-supercritical profile

We further investigate the large distance behavior of profile solutions following (Ref. 21, Proposition 7.1).

Proposition 1. *As $\xi \to \infty$ solutions of (16) behave asymptotically as $Q = \alpha Q_1 + \beta Q_2$, where*

$$Q_1(\xi) \approx |\xi|^{-\frac{i}{a}-\frac{1}{\sigma}}, \qquad Q_2(\xi) \approx e^{-\frac{ia\xi^2}{2}}|\xi|^{-\frac{i}{a}-d+\frac{1}{\sigma}}, \quad \alpha, \beta \in \mathbb{C}. \tag{28}$$

Proof. Substituting $Q(\xi) = e^{-ia\xi^2/4}\xi^{(1-d)/2}Z(\xi)$ into (16), we obtain

$$-Z'' + \left(-\frac{a^2}{4}\xi^2 + 1 - ia\, s_c + \frac{(d-1)(d-3)}{4\xi^2}\right.$$
$$\left.-((-\Delta)^{-1}|\xi|^{\frac{(1-d)}{2}(2\sigma+1)}|Z|^{2\sigma+1})|\xi|^{\frac{(1-d)}{2}(2\sigma-1)}|Z|^{2\sigma-1}\right) Z = 0.$$

Writing $Z(\xi) = e^{w(\xi)}$, yields

$$w'' + (w')^2 + \frac{a^2}{4}\xi^2 - 1 + ia \quad s_c - \frac{(d-1)(d-3)}{4}\xi^{-2} = O(e^{2\sigma w}|\xi|^{-2\sigma(d-1)+2}). \tag{29}$$

Now, for $s_c \geq \frac{1}{2}$, we can drop the nonlinear term $((-\Delta)^{-1}|Q(s)|^{2\sigma+1})|Q(s)|^{2\sigma-1}Q$ to compute the asymptotics, which gives two linear independent solutions

$$w_1 \sim ia\frac{\xi^2}{4} - \frac{i}{a}\ln|\xi| - \left(\frac{1}{2} - s_c\right)\ln|\xi|,$$
$$w_2 \sim -ia\frac{\xi^2}{4} + \frac{i}{a}\ln|\xi| + \left(\frac{1}{2} - s_c\right)\ln|\xi|.$$

Returning back to the notation of Q, we get (28).

We note that if $s_c < \frac{1}{2}$, then the term with ξ^{-2} in (29) is not dominant compared with the right side. For conciseness we only consider $s_c \geq \frac{1}{2}$, it is also the setting we use in our numerical study below. ■

We note that Q_2 is the fast oscillating solution as $\xi \to \infty$, which we should exclude from Q (or require that $\beta = 0$), since we are interested in complex-valued solutions Q, which have monotonically decreasing amplitude $|Q|$, of the form αQ_1. Such solutions are typically referred to as "admissible solutions." More importantly, excluding the span of Q_2 gives us solutions with finite Hamiltonian.

Proposition 2. *If Q is a solution of (16) with $Q_\xi \in L^2(\mathbb{R}^d)$ and $Q \in L^{\frac{2d(2\sigma+1)}{(d+2)}}(\mathbb{R}^d)$, and $s_c \neq 0$, its Hamiltonian is a nonzero constant, that is,*

$$\int \left(|Q_\xi|^2 - \frac{1}{2\sigma+1} V(Q) \right) \xi^{d-1} d\xi = const, \tag{30}$$

where $V(Q)$ is defined in (19).

Equivalently, taking $P = e^{ia\xi^2/4} Q$, yields

$$\int \left(|P_\xi|^2 - \frac{1}{2\sigma+1} V(Q) + a \operatorname{Im}(\xi P \bar{P}_\xi) + \frac{a^2 \xi^2}{4} |P|^2 \right) \xi^{d-1} d\xi = const. \tag{31}$$

Proof. As in the proof of Lemma (1), multiply (16) by ΔQ and apply (21), (22) with $\xi \to \infty$. Note that $Q \in L^{\frac{2d(2\sigma+1)}{(d+2)}}(\mathbb{R}^d)$, since $Q(\xi) \sim \xi^{-1/\sigma}$, and the Hardy-Littlewood inequality implies $V(Q) \in L^1_{\text{rad}}(\mathbb{R}^d)$. Since

$$a \left[\left(\frac{d}{2} - \frac{1}{\sigma} - 1 \right) \left(\int \left(|Q_\xi|^2 - \frac{1}{2\sigma+1} V(Q) \right) \xi^{d-1} d\xi \right) - \frac{1}{2\sigma+1} \int V(Q) \xi^{d-1} d\xi \right] = 0 \tag{32}$$

with the last term being a constant, we obtain that the first term is also a constant, provided $s_c \neq 1$, completing the proof. ■

Remark 4. From the identity (32), we note that the energy of Q is not necessarily zero when $0 < s_c < 1$. Our numerical calculations show that, for example, in the 3D gHartree case with $\sigma = 1$ ($p = 3$), we get $E[Q] \approx 0.96$. This is different from the NLS case. However, we will show that this does not affect obtaining the *log-log* blow-up rate in the L^2-critical case (see Section 4).

2.3.1 | Admissible solutions to (13)

To discuss what happens with admissible solutions in the case when $s_c = 0$ (more precisely, $s_c \searrow 0$), we allow flexibility by letting the dimension d vary continuously (as in Ref. 21) so that Equation (16) becomes slightly L^2-supercritical. The reason for this flexibility is to investigate existence of solutions to (16) when $s_c = 0$; in particular, if we stay rigid in this case with the nonlinearity $\sigma = 2/d$, then Equation (16) does not have reasonable solutions when $a \neq 0$.

Proposition 3. *Equation (16) with $\sigma = \frac{2}{d}$ ($s_c = 0$) has no admissible solutions when $a \neq 0$ and a is finite.*

Proof. We split Q into the real amplitude and phase by writing $Q = We^{i\theta}$. Equation (16) produces the following system for functions $W(\xi)$ and $\theta(\xi)$:

$$\Delta W - W + \left((-\Delta)^{-1}|W|^{2\sigma+1}\right)|W|^{2\sigma-1}W - \theta_\xi(a\xi + \theta_\xi) = 0, \tag{33}$$

$$\frac{\partial}{\partial\xi}\left(\xi^{\frac{2}{\sigma}-1}W^2\left(\theta_\xi + \frac{a}{2}\xi\right)\right) + \frac{\sigma d - 2}{\sigma}\,\xi^{\frac{2}{\sigma}-2}\theta_\xi\, W^2 = 0. \tag{34}$$

Note that the nonlinearity only shows up in the first equation, while the existence of admissible solutions comes from examining the second equation, where the second term vanishes when $\sigma = 2/d$, giving $\theta(\xi) = -a\xi^2/4$. Now using the large distance behavior from (28), and giving the same argument as in the NLS case (Ref.[21], section 8.1.1), the conclusion that there are no admissible solutions for $a \neq 0$ in the L^2-critical case $\sigma = \frac{2}{d}$ (or when dimension $d = \frac{2}{\sigma}$) follows. ∎

Remark 5. This seems to be the feature for any L^2-critical NLS-type equation with *any* nonlinear term (as long as $\sigma = \frac{2}{d}$).

Remark 6. If $a = 0$, then (16) becomes $\Delta Q - Q + ((-\Delta)^{-1}|Q|^{2\sigma+1})|Q|^{2\sigma-1}Q = 0$, which is exactly (8). Thus, the solutions of (13) convergence in some sense to ground state solutions of (13).

We are now ready to investigate the behavior of blow-up solutions, and in particular, behavior of the parameter $a(\tau)$. We start with the description of the dynamic rescaling method needed for the gHartree equation.

3 | THE DYNAMIC RESCALING METHOD

The dynamic rescaling method, which was first introduced in Ref. 30 in 1986, has proven to be an efficient way to simulate the blow-up phenomena for the NLS equation. As the generalized Hartree has scaling symmetry, we apply a similar approach and study (16), in particular, we recall the parameter $L(t)$ from (14). We note that the proper choice for representing $L(t)$ will provide the global existence of the rescaled equation (13) on τ. Recall that the blow-up rate is defined, for example, as $\|\nabla u(t)\|_2 \sim f(t)$ for some function $f(t)$. Direct calculation by the chain rule from (12) shows

$$\|\nabla u(t)\|_2 = \frac{1}{L(t)^{\frac{1}{2}(1-s_c)}}\|\nabla v(\tau)\|_2, \tag{35}$$

and thus, the behavior of $L(t)$ describes the rate of the blow-up. As we discussed in Ref. 22, one intuitive choice for $L(t)$ is to restrict the norm $\|\nabla v\|_2$ to be constant in time, that is,

$$L(t) = \left(\frac{\|\nabla v_0\|_2^2}{\|\nabla u(t)\|_2^2}\right)^\beta.$$

The direct calculation leads to

$$\beta = \frac{1}{2/\sigma + 2 - d},$$

and

$$a(\tau) = -\frac{2\beta}{\|\nabla v_0\|_2^2} \mathrm{Im}\left(\int_0^\infty \left((-\Delta)^{-1} |v|^{2\sigma+1} \right) |v|^{2\sigma-1} \bar{v} \Delta v \xi^{d-1} d\xi \right). \tag{36}$$

An alternative choice for $L(t)$ (from Definition 2) is to restrict the L^∞ norm of the solution to the rescaled equation $v(\tau)$ to be constant, say $\|v(\tau)\|_{L^\infty} = 1$ (as we mentioned in the introduction, the blow-up rate in the L^∞ norm is equivalent to the blow-up in the $\dot{H}^1$ norm, see also Refs. 11, 25). By setting

$$L(t) = \left(\frac{1}{\|u(t)\|_\infty} \right)^\sigma, \tag{37}$$

one has

$$a(\tau) = -\sigma \ \mathrm{Im}(\bar{v} \Delta v)(0, \tau). \tag{38}$$

In this work, we fix $\|v(\tau)\|_\infty \equiv 1$ instead of $\|\nabla v\|_2$, since computing the last norm involves the integral $\int_0^\infty \cdots \xi^{d-1} d\xi$ for $d > 1$ (we will consider $d = 3, 4, 5, 6, 7$); when the dimension d becomes higher, say $d = 7$, the values of the term $\int_0^\infty \cdots \xi^{d-1} d\xi$ in (36) become very large. If we fix $\|v\|_{L^\infty}$, then there will be no influence on $a(\tau)$ from the dimension d. Actually, both options lead to the same results in the cases $d = 3$ and $d = 4$ (lower dimensions). For the L^2-supercritical case, which we consider in Section 4, we choose to fix the value $\|v(\tau)\|_\infty$ to be constant; this is in part because when $s_c > 1$, Definition 1 has to be replaced with the blow-up rate defined with respect to the $\dot{H}^s$ norm for $s > s_c$, that is,

$$\lim_{t \nearrow T} \frac{\|u(t)\|_{\dot{H}^s}}{f(t)} = C$$

for some function $f(t)$.

We return to Equation (13), which is of the form

$$i v_\tau + \Delta v + \mathcal{N}(v) = 0, \tag{39}$$

where $\mathcal{N}(v) = ia(\tau)(\xi v_\xi + \frac{v}{\sigma}) + ((-\Delta)^{-1}|v|^{2\sigma+1})|v|^{2\sigma-1}v$.

Equation (39) is of the same form as the one we studied in Refs. 22 and 23. It is given on the whole space $\xi \in [0, \infty)$, and for numerical purposes, we ought to map the spatial domain $[0, \infty)$ onto some finite interval, for example, onto $[-1, 1)$. For that, we choose the mapping from Ref. 30, by setting $\xi = l \frac{1+z}{1-z}$. Here, l is a constant indicating the half number of the collocation points assigned on the interval $[0, l]$ and z is the Chebyshev-Gauss-Lobatto collocation points from $[-1, 1]$ (see Ref. 51). We impose the homogeneous Dirichlet boundary condition, $v(\infty) = 0$, on the right, and thus, we remove the last Chebyshev point, and, consequently, delete the last row and the last column of the matrix $\mathbf{M}$ in (42). The Laplacian operator can be discretized from the Chebyshev-Gauss-Lobatto differentiation matrix (refer to Refs. 51 and 52 for details). We denote the discretized

Laplacian with $N+1$ collocation points by the matrix Δ_N. The nonlocal operator $(-\Delta)^{-1}$ can now be approximated by the matrix $(-\Delta_N)^{-1}$, which is the inverse of the matrix $-\Delta_N$ with the first row replaced by the first row of the Chebyshev differential matrix because of the Neumann homogeneous boundary condition, $\varphi_\xi(0)=0$, for the equation $-\Delta\varphi = |\upsilon|^{2\sigma+1}$ for the nonlocal term. This also avoids the singularity of the Laplacian at $\xi=0$. The matrix $(-\Delta)_N^{-1}$ needs to be calculated only once by numerically taking the inverse of the matrix $-\Delta_N$ and then storing it to be used later to calculate the time evolution.

To discuss the time evolution, we use the following notation for υ as the semi-discretization in time variable τ: let $\upsilon^{(m)} \approx \upsilon(\xi, m\cdot\Delta\tau)$ be the approximation of υ at the time $m\cdot\Delta\tau$, where $\Delta\tau$ is the time step and m is the number of iterations. The time evolution of (39) can be approximated by the second-order Crank-Nicolson-Adam-Bashforth method, that is,

$$i\frac{\upsilon^{(m+1)}-\upsilon^{(m)}}{\Delta\tau} + \frac{1}{2}\left(\Delta\upsilon^{(m+1)} + \Delta\upsilon^{(m)}\right) + \frac{1}{2}\left(3\mathcal{N}(\upsilon^{(m)}) - \mathcal{N}(\upsilon^{(m-1)})\right) = 0. \tag{40}$$

We rewrite (40) as

$$\left(\frac{i}{\Delta\tau} + \frac{1}{2}\Delta\right)\upsilon^{(m+1)} = \left(\frac{i}{\Delta\tau} - \frac{1}{2}\Delta\right)\upsilon^{(m)} - \frac{1}{2}\left(3\mathcal{N}(\upsilon^{(m)}) - \mathcal{N}(\upsilon^{(m-1)})\right). \tag{41}$$

With the Laplacian operator Δ replaced by the matrix Δ_N, and also the term $\frac{i}{\Delta\tau}$ replaced by the diagonal matrix $\mathbf{diag}(\frac{i}{\Delta\tau})$, equation (41) is equivalent to the following linear system:

$$\mathbf{M}\upsilon^{(m+1)} = \mathbf{F}(\upsilon^{(m)}, \upsilon^{(m-1)}). \tag{42}$$

Therefore, each time step is updated by

$$\upsilon^{(m+1)} = \mathbf{M}^{-1}\mathbf{F}(\upsilon^{(m)}, \upsilon^{(m-1)}).$$

Again, the inverse of the matrix $\mathbf{M}$ can be calculated and stored only once in the beginning, since $\mathbf{M} = (\mathbf{diag}(\frac{i}{\Delta\tau}) + \frac{1}{2}\Delta_N)$ stays the same.

The boundary conditions are imposed similar to Refs. 22, 30, 51 and 52 as follows: For the homogeneous Neumann boundary condition on the left, $\upsilon_\xi(0)=0$, we substitute the first row of the matrix $\mathbf{M}$ by the first row of the first-order Chebyshev differential matrix, and change the first element of the vector $\mathbf{F}$ to 0. Because of the homogeneous Dirichlet boundary condition $\upsilon(\infty)=0$ on the right, we delete the last row and column of $\mathbf{M}$ as well as the last element of the vector $\mathbf{F}$.

The mapped Chebyshev collocation discretization gives us spectral accuracy in space. Figure 1 shows that the coefficients reach the machine accuracy (10^{-16}) within 200 grid points. Note that the Chebyshev coefficients and derivative terms in $\mathbf{F}(\upsilon^{(m)}, \upsilon^{(m-1)})$ can be evaluated by the fast Fourier transform (FFT). To utilize the FFT efficiently, we use $N=256$ grid points (instead of 200).

After each $\upsilon^{(m+1)}$ is obtained, the terms $a^{(m+1)}$ and $\ln L(\tau_{m+1})$ can be updated by the trapezoidal rule:

$$\ln L(\tau_{m+1}) = \ln L(\tau_m) + \frac{\Delta\tau}{2}(a^{(m+1)} + a^{(m)}). \tag{43}$$

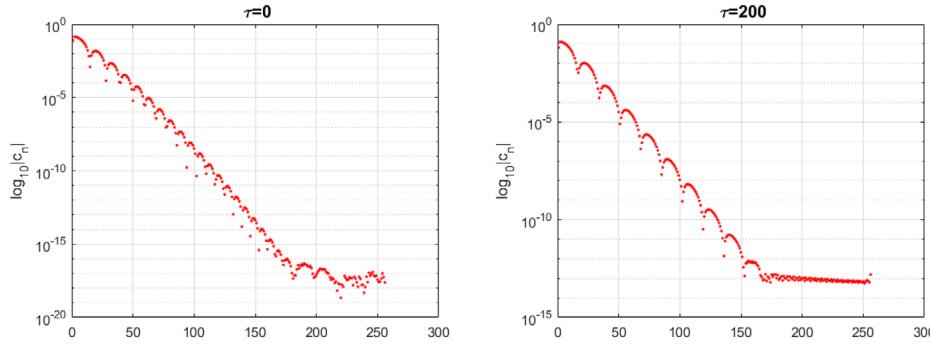

FIGURE 1 The 4D case: the Chebyshev coefficients for the solution $v(\xi, \tau)$ at $\tau = 0$ (left) and $\tau = 200$ (right)

To determine the blow-up rate, we track the quantity $T - t$ (and then compute $\ln(T - t)$) in a similar way as we did in Refs. 22 and 23. The RHS of (43) produces from the mth step the value $\ln L(\tau_{m+1})$ on the LHS; exponentiating it, we get $\exp(\ln L(\tau_{m+1}))$, which is the value of $L(\tau_{m+1})$. Now, denoting $\Delta t_{m+1} := t_{m+1} - t_m$, we obtain this difference from the last equation of (12)

$$\Delta t_{m+1} = \Delta\tau L^2(\tau_{m+1}). \tag{44}$$

Hence, starting from $t_0 = 0$, the mapping for the rescaled time τ back to the real time t is calculated as

$$t(\tau_{m+1}) = \sum_{j=1}^{m+1} \Delta t_j = \Delta\tau \sum_{j=1}^{m+1} L(\tau_j)^2. \tag{45}$$

Note that as time evolves, the time difference $T - t(\tau_n)$ will become smaller and smaller, and eventually reach saturation level (with little change), therefore, we treat the stopping time $t(\tau_{\text{end}}) = t(\tau_M)$ as the blow-up time T, where M is the total number of iterations when reaching the stopping condition ($L < 10^{-24}$). Then, we can take

$$T = t(\tau_{\text{end}}) = \Delta\tau \sum_{j=1}^{M} L(\tau_j)^2. \tag{46}$$

Consequently, for any t_i, we calculate $T - t_i$ as

$$T - t_i = \sum_{j=i+1}^{M} \Delta t_j = \Delta\tau \sum_{j=i+1}^{M} L(\tau_j)^2. \tag{47}$$

This indicates that instead of recording the cumulative time t_i, we only need to record the elapsed time between the two recorded data points, that is, $\Delta t_{i+1} = t_{i+1} - t_i$. By doing so, we avoid the loss of significance when adding a small number onto a large one.

Since the mapped-Chebyshev collocation method may suffer from the under-resolution issue (when the solution is far away from the origin), we also use the finite difference method with the uniform mesh size on a bounded domain. This involves constructing the artificial boundary

conditions to approximate $v(\infty) = 0$ as well as the nonlocal term $((-\Delta)^{-1}|v|^{2\sigma+1})|v|^{2\sigma-1}v$ at $\xi = \infty$. Similar to the argument in Ref. 21, we know that the terms Δv and $((-\Delta)^{-1}|v|^{2\sigma+1})|v|^{2\sigma-1}v$ are of the higher order compared with the remaining linear terms in (13). When $\xi \gg 1$, these two terms can be negligible and Equation (13) reduces to

$$v_\tau + a(\tau)\big(\alpha v + \xi v_\xi\big) = 0 \quad \text{at} \quad \xi = K, \tag{48}$$

where K is our computational domain length taken to be large enough. The equation (48) can be solved exactly

$$v(\xi,\tau) = v_0\left(\xi\frac{L(\tau)}{L(0)}\right)\left(\frac{L(\tau)}{L(0)}\right)^{\frac{1}{\sigma}}. \tag{49}$$

This suggests that at $\xi = K$, we have

$$v(K,\tau_{m+1}) = v\left(K\frac{L(\tau_{m+1})}{L(\tau_m)}\right)\left(\frac{L(\tau_{m+1})}{L(\tau_m)}\right)^{\frac{1}{\sigma}}. \tag{50}$$

The $L(\tau_{m+1})$ can be approximated by the second-order central difference

$$L(\tau_{m+1}) = L(\tau_{m-1}) + 2\Delta\tau L_\tau(\tau_m).$$

Note that $a^{(m)} = -\frac{L_\tau(\tau_m)}{L(\tau_m)}$, and $\frac{L(\tau_m)}{L(\tau_{m-1})}$ can be approximated by $\frac{L(\tau_m)}{L(\tau_{m-1})} = e^{-\frac{\Delta\tau}{2}(a^{(m-1)}+a^{(m)})} + O(\Delta\tau^3)$. Therefore, the right side boundary condition is approximated with second-order accuracy

$$v(K,\tau_{m+1}) = v\left(K(e^{+\frac{\Delta\tau}{2}(a^{(m-1)}+a^{(m)})} - 2\Delta\tau a^{(m)})\right)\left((e^{+\frac{\Delta\tau}{2}(a^{(m-1)}+a^{(m)})} - 2\Delta\tau a^{(m)})\right)^{\frac{1}{\sigma}}. \tag{51}$$

We also discretize Equation (39) by a uniform mesh with the boundary condition (51). Let $v(\xi_j,\tau) \approx v(jh,\tau)$ to be the semi-discretization in space, where $h = \xi_{j+1} - \xi_j$ is the spatial grid size, the derivatives are approximated by the sixth-order central difference:

$$v_\xi(jh,\tau) \approx D_6^{(1)}v_j = \frac{1}{60h}[-v_{j-3} + 9v_{j-2} - 45v_{j-1} + 45v_{j+1} - 9v_{j+2} + v_{j+3}],$$

$$v_{\xi\xi}(jh,\tau) \approx D_6^{(2)}v_j = \frac{1}{180h^2}[2v_{j-3} - 27v_{j-2} + 270v_{j-1} - 490v_j + 270v_{j+1} - 27v_{j+2} + 2v_{j+3}],$$

and the Laplacian operator is approximated by

$$\Delta v(jh,\tau) \approx \Delta_h v_j = v_{\xi\xi}(jh,\tau) + \frac{d-1}{jh}v_\xi(jh,\tau). \tag{52}$$

In fact, we also tested our approach with the second-order and fourth-order central difference method, and obtained the consistent result. The reported results are obtained by the sixth-order central difference method.

When the grid points beyond the right side computational domain are needed, we set up the fictitious points obtained by extrapolation

$$v_{N+2} = 8v_{N+1} - 28v_N + 56v_{N-1} - 70v_{N-2} + 56v_{N-3} - 28v_{N-4} + 8v_{N-5} - v_{N-6}.$$

For the grid points beyond the left side computational domain, note that $v(\xi)$ is radially symmetric, and thus, we use the fictitious points $v_{-j} = v_j$. The singularity at $\xi = 0$ in the Laplacian term Δ_h is eliminated by the L'Hospital's rule

$$\lim_{\xi\to 0} \frac{d-1}{\xi} v_\xi = (d-1)v_{\xi\xi}.$$

As in Ref. 22, for the NLS equation, we have an alternative way to approximate the time evolution by introducing a *predictor-corrector* scheme (see also Ref. 19):

$$i\frac{v_{\text{pred},j}^{(m+1)} - v_j^{(m)}}{\Delta\tau} + \frac{1}{2}\left(\Delta_N v_{\text{pred},j}^{(m+1)} + \Delta_N v_j^{(m)}\right) + \frac{1}{2}\left(3\mathcal{N}(v_j^{(m)}) - \mathcal{N}(v_j^{(m-1)})\right) = 0, \quad \text{(P)} \tag{53}$$

$$i\frac{v_j^{(m+1)} - v_j^{(m)}}{\Delta\tau} + \frac{1}{2}\left(\Delta_N v_j^{(m+1)} + \Delta_N v_j^{(m)}\right) + \frac{1}{2}\left(\mathcal{N}(v_{\text{pred},j}^{(m+1)}) + \mathcal{N}(v_j^{(m-1)})\right) = 0. \quad \text{(C)} \tag{54}$$

Both approaches (40) and (53)-(54) lead to similar results. Numerical tests suggest that (53) and (54) is slightly more accurate than the scheme (40), though it is still a second-order scheme in time and it doubles the computational time, therefore, we mainly use the *predictor-corrector* scheme (53) and (54) in our simulation.

We next remark about the term $|v|^{p-2}$. The power $p-2$ may become negative in the L^2-critical case when $d \geq 5$ (since $p = 1 + \frac{4}{d} < 2$). Numerically, this may cause problems as the singularities may occur if $v(\xi_0, \tau) = 0$ at certain points ξ_0. To avoid this issue, we write $v = |v|e^{i\theta}$, hence, the outside nonlinear term becomes

$$|v|^{p-2}v = |v|^{p-2}|v|e^{i\theta} = |v|^{p-1}e^{i\theta}. \tag{55}$$

Note that with (55), we can deal with $p \geq 1$, in particular, $p = 1 + \frac{4}{d}$. Furthermore, we can also use v when it is zero, by defining

$$\left((-\Delta)^{-1}|v|^p\right)|v|^{p-2}v = \begin{cases} \left((-\Delta)^{-1}|v|^p\right)|v|^{p-2}v & \text{if } |v| > 0 \\ 0 & \text{if } |v| = 0, \end{cases} \tag{56}$$

since zeros occurring on the term $|v|^{p-2}v$ are of the higher order term compared with the zeros occurring on v.

We set the rescaled initial value $\|v_0\|_\infty = 1$. We choose $N = 256$ collocation points, the mapping parameter $l = 256$, and $\Delta\tau = 2 \times 10^{-3}$, if we apply the mapped collocation spectral method to work on the entire space. Alternatively, we choose $h = 0.1$, $K = 120$, and $\Delta\tau = 10^{-4}$, if we use the finite difference method and apply the artificial boundary condition (51). Again, these two discretizations lead to similar results. Initially, we only have $v^{(0)} = v_0$. The next time step $v^{(1)}$ can be obtained by the standard second-order explicit Runge-Kutta method (RK2).

TABLE 1 Various values for the initial condition $u_0 = A_0 e^{-\frac{r^2}{d}}$ depending on the dimension d

d	A_0	$\tilde{A}$ (threshold)	$\|e^{-\frac{r^2}{d}}\|_2^2$	$\|Q\|_2^2$
3	4	1.9878	0.81405	3.2167
4	5	2.774	2	15.3898
5	6	3.7019	6.5683	90.0122
6	7	4.8631	27	638.5311
7	8	6.3399	133.2859	5357.3174

Note. Here, $\|Q\|_2^2$ is the mass of the ground state, the value $\tilde{A}$ gives the threshold for the finite time blow-up versus globally existing solutions, A_0 is an example of the amplitude used. For reference, the L^2-norm of $e^{-\frac{r^2}{d}}$ is also listed. Note that $\tilde{A}^2 \cdot \|e^{-\frac{r^2}{d}}\|_2^2 \approx \|Q\|_2^2$. (All of the L^2-norms are calculated without the dimensional constant $\alpha(d)$.)

TABLE 2 The error for the conserved quantity $\|v(\tau)\|_\infty$ in τ by using the predictor-corrector method with $\delta\tau = 2 \times 10^{-3}$ with respect to the dimension d

d	3	4	5	6	7
$\mathcal{E}$	8×10^{-9}	7×10^{-9}	4×10^{-9}	2×10^{-9}	2×10^{-9}

4 | THE L^2-CRITICAL CASE

In this section, we only consider the L^2-critical case, that is, $\sigma = 2/d$ and

$$iu_t + \Delta u + \left((-\Delta)^{-1}|u|^{1+\frac{4}{d}}\right)|u|^{\frac{4}{d}-1}u = 0, \quad d \geq 3.$$

4.1 | Preliminary investigation of rates and profile

4.1.1 | Initial data

Similar to the NLS equation in Refs. 22 and 30, we use the Gaussian-type initial data $u_0(r) = Ae^{-r^2}$, which leads to the self-similar blow-up solutions concentrated at the origin. As the amplitude A_0 can become very large in higher dimensions, we normalize the exponent and work with data $u_0 = A_0 e^{-\frac{r^2}{d}}$, since the normalization term $\frac{r^2}{d}$ keeps A_0 reasonably small. Table 1 lists the mass of the ground state Q, the mass of $e^{-\frac{r^2}{d}}$, and we also list the threshold of the amplitude $\tilde{A}$ for the finite time blow-up solutions versus globally existing solutions. The amplitude A_0 is one of the examples from our simulation (one could choose any $A_0 > \tilde{A}$). We remark that we drop the dimensional constant $\alpha(d)$ in our calculations.

To demonstrate the precision of our calculations, we check the following quantity $\|v(\tau)\|_{L_\xi^\infty}$, which is supposed to be conserved in time τ. Table 2 shows how this quantity $\|v\|_{L_\xi^\infty}$ varies in the rescaled time τ, that is, $\mathcal{E} = \max_\tau(\|v(\tau)\|_{L_\xi^\infty}) - \min_\tau(\|v(\tau)\|_{L_\xi^\infty})$, which is at least on the order of 10^{-7}.

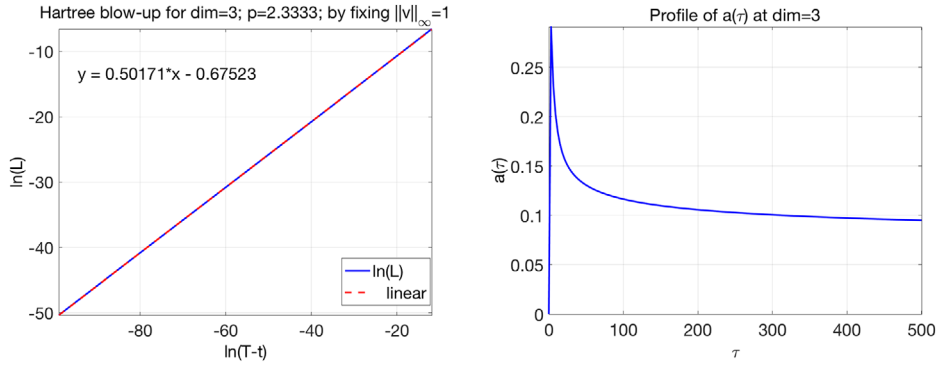

FIGURE 2 3D ($p = \frac{7}{3}$): the slope of $L(t)$ versus $T - t$ on a *log* scale, which shows the slope of $\frac{1}{2}$ (left); the behavior of $a(\tau)$—very slow decay (right)

4.1.2 | Blow-up rate

In this part we investigate behavior of $L(t)$. We plot the slope of $\ln L$ versus $\ln(T - t)$ and dependence of $a(\tau)$ on τ in dimensions $d = 3, \dots, 7$ in Figures 2 and 3. The subplots on the left show that the slope is approximately $\frac{1}{2}$ (e.g., the slope of $\ln(T - t)$ versus $\ln L$ is 0.50171 in 3D). The subplots on the right show a (slow) decay of the coefficient $a(\tau)$, recall this coefficient from (13) and (14). Note that $a(\tau)$ decays very slowly in τ, this is similar to the decay of the corresponding $a(\tau)$ in the L^2-critical NLS equation in Refs. 22 and 30 We also plot the dependence of $a(\tau)$ versus $1/(\ln(\tau) + 3\ln\ln\tau)$, and observe that it fits the straight line very well (see Figure 4), here we are using the same expression in the denominator for the consistency with the NLS computations and fittings (see more discussion on this below).

Because of the second term in the above fitting (in Figure 4), one might expect that the correction term in the blow-up rate should be the *log-log* correction. We may also expect that the self-similar blow-up solution converges to the ground state profile Q (up to scaling) as $a(\tau) \to 0$ from the slow decay of $a(\tau) \sim 1/(\ln(\tau) + 3\ln\ln\tau)$. In the next two subsections, we confirm these implications, that is, the convergence of blow-up profiles to the ground state Q, and also provide justifications to the *log-log* correction.

Remark 7. In the following subsections, we study the decay rate of $a(\tau)$ via the *asymptotic analysis*. We obtain that at the first leading order, as $\tau \to \infty$, $a(\tau)$ decays at the rate $\frac{\pi}{\ln\tau}$, that is, slower than any polynomial rate. When in asymptotic analysis more corrective terms are retained, then one can get $a(\tau) \sim \pi/(\ln\tau + c \cdot \ln\ln\tau)$, and $a_\tau \sim -a^{-1}e^{-\pi/a}$ yields $c = 3$. This is why in our numerical figures (e.g., in Figure 4) we only show the dependence of $a(\tau)$ versus $1/(\ln\tau + 3\ln\ln\tau)$ in this paper. We note that when we change the constant c in the second term of $1/(\ln\tau + c\ln\ln\tau)$ with different values of c, including zero and large constants (we tried with $c = 0, 1, 3, 100, 1000$), we find that the slope does not change much, which only confirms that such a correction is difficult to track numerically as it only happens at the very high focusing levels. See Refs. 39, 40 for the results beyond the empirical term $1/(\ln\tau + c\ln\ln\tau)$.

We next note that the slope of the line is not $\frac{1}{\sqrt{2\pi}}$ as expected from the asymptotic analysis, where the correction term for $a(\tau)$ is given by $q(t) \sim ((2\pi)/\ln\ln(\frac{1}{T-t}))^{1/2}$. This is because at the time we terminate our simulations, which we are forced to do as the maximal current numerical

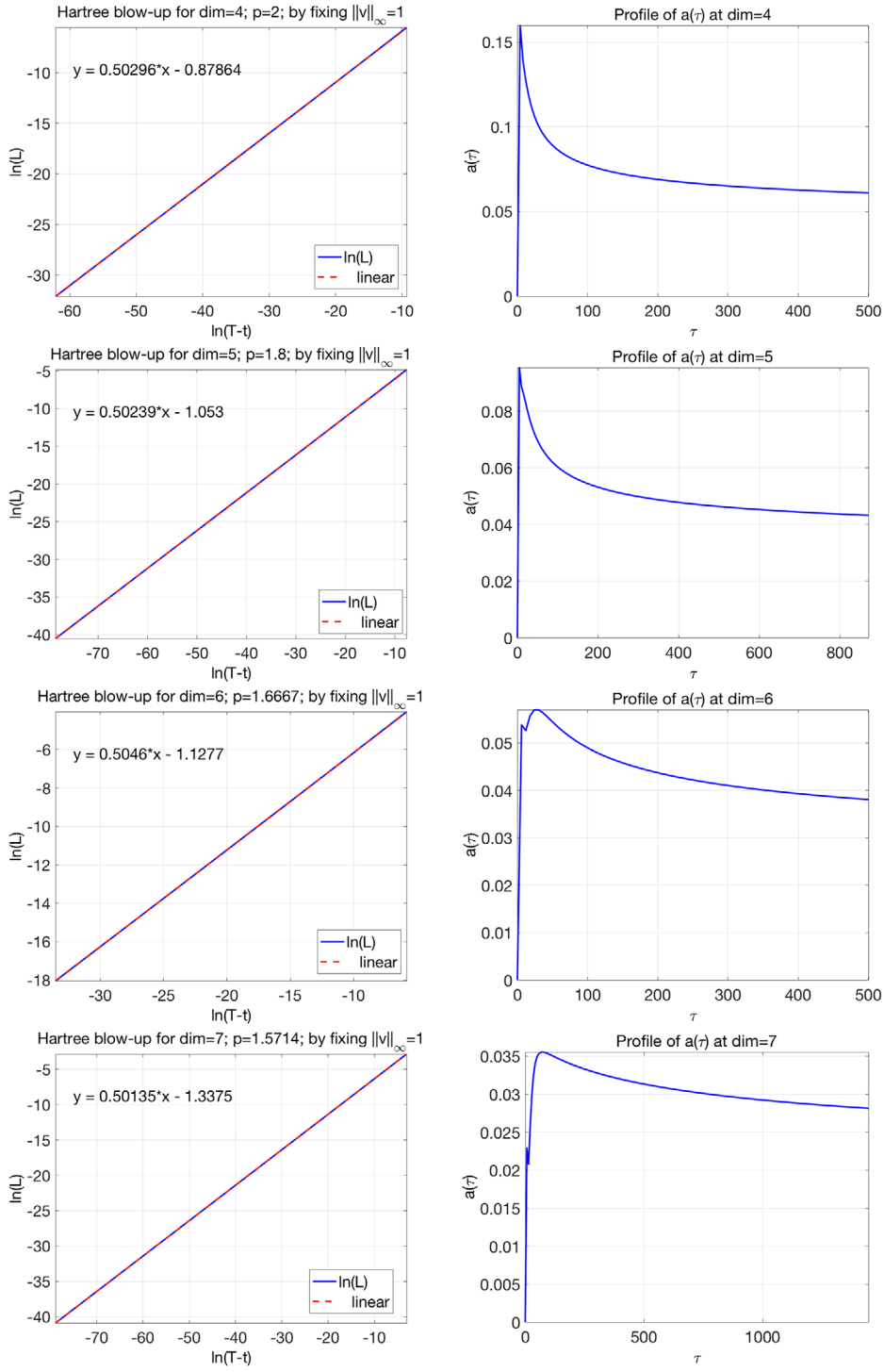

FIGURE 3 The slope of $L(t)$ versus $T-t$ on a *log* scale (left); the slow decay of $a(\tau)$ (right). Top: 4D ($p=2$); Top middle: 5D ($p=\frac{9}{5}$); Bottom middle: 6D ($p=\frac{5}{3}$); Bottom: 7D ($p=\frac{11}{7}$)

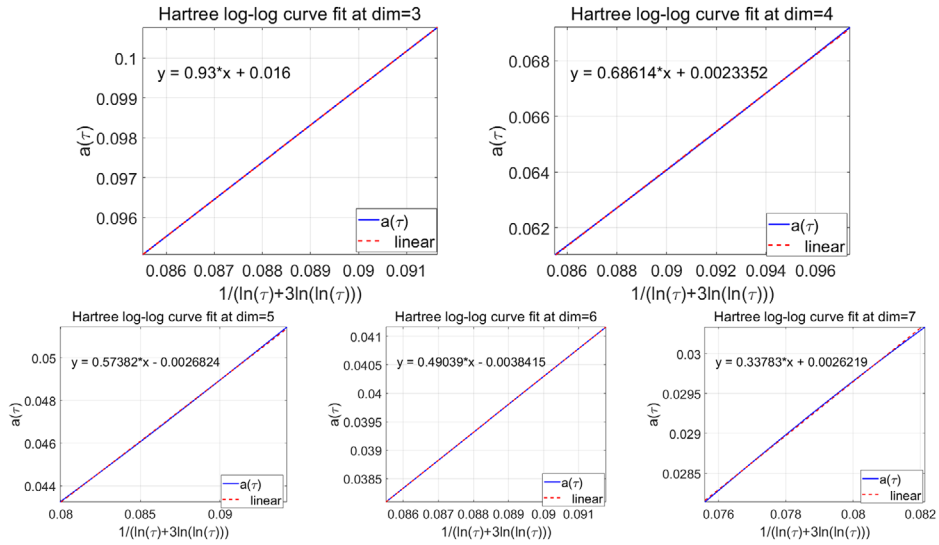

FIGURE 4 Fitting for $a(\tau)$ versus $1/(\ln\tau + 3\ln\ln(\tau))$

TABLE 3 The values of $\| v(\tau) - Q\|_\infty$, where $v(\tau)$ is the solution to the rescaled equation (13)

d	$\tau = 0$	$\tau = 10$	$\tau = 50$	$\tau = 100$	$\tau = 200$	$\tau = 400$
3	0.3267	0.0325	0.0136	0.0106	0.0086	0.0072
4	0.2402	0.03331	0.0122	0.0089	0.0070	0.0057
5	0.1878	0.0290	0.0120	0.0085	0.0064	0.0051
6	0.1497	0.0218	0.0119	0.0087	0.0065	0.0051
7	0.1188	0.0118	0.0102	0.0082	0.0065	0.0052

Note. The values are decreasing as $\tau \to \infty$, or equivalently, $t \to T$.

precision is reached, the values of $a(\tau)$ are still far from 0, similar to the computations for the NLS equation in Refs. 20, 22, 50. These facts indicate that the *log-log* regime occurs only when the amplitude is very large (say $\gg 10^{200}$).

4.1.3 | Blow-up profiles

In this part, we investigate the profiles of blow-up solutions at the time $\tau = 2, 40, 200, 400$ in dimension $d = 3, \dots, 7$. Figures 5 and 6 show plots of $|v(\xi, \tau)|$ and $|u(r, t)|$ next to each other as we plot in pairs different times τ and the corresponding t, recalling that v is the solution to the rescaled equation (12) and u is the solution to the gHartree equation (6) reconstructed from v. These figures demonstrate that the blow-up solutions $v = v(\xi, \tau)$ converge to the rescaled ground state profile Q from (8), or (7), in all dimensions we simulated ($d = 3, \dots, 7$). (The Appendix explains the computation of Q via the renormalization method.) Table 3 shows that $\| v(\tau) - Q\|_\infty \to 0$ as $\tau \to \infty$, but very slowly, which matches our hypothesis about slow decay of $a(\tau)$. This confirms that the blow-up profile $u(x, t)$ converges to Q, that is, $\| u(t) - Q\|_\infty \to 0$ as $t \to T$, up to scaling.

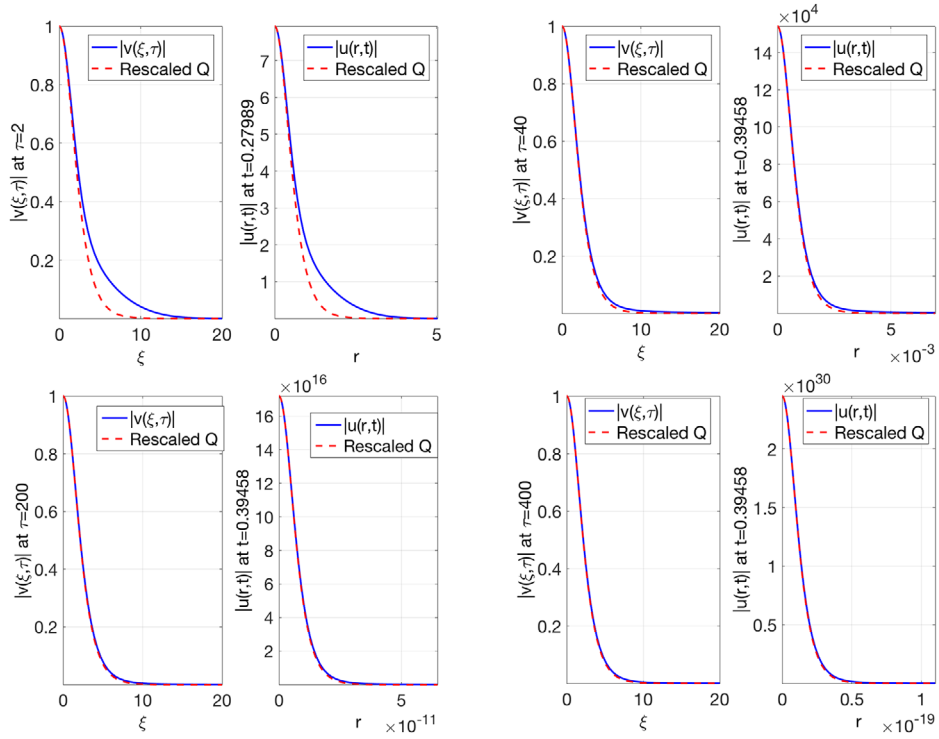

FIGURE 5 Convergence of blow-up profile in the dimension $d = 3$. Next to each other we plot the rescaled profile $|v|$ in the rescaled time τ and the original solution $|u|$ in the actual time t. As $\tau \to \infty$ (here, $\tau = 2, 40, 200, 400$), the profile (blue dots) approaches the rescaled ground state Q, that is, $Q_{\text{rescaled}} = \frac{1}{L^a(t)} Q(\frac{r}{L(t)})$

4.2 | First attempt to obtain the correction term in the blow-up rate

In the NLS equation, the *log-log* regime is reached when the amplitude of the solution is extremely large ($\gg 10^{200}$), which is currently impossible to observe numerically. In Ref. 38, the functional form testing was suggested and the authors succeeded in showing that among all tested functional forms, the *log-log* form minimizes the errors in the fitting the best. This method has also been proven to be efficient in checking the *log-log* correction for the NLS equation in higher dimensions, see Ref. 22. In this paper, we also use this approach for the correction term in the blow-up rate in the gHartree equation. We write the rate as

$$\frac{1}{L(t)} \sim \left(\frac{F(T-t)}{T-t} \right)^{\frac{1}{2}}, \tag{57}$$

where $F(s) = (\ln(s^{-1}))^{\gamma}$ (e.g., we consider $\gamma = 1, 0.6, 0.5, 0.4, 0$) or $F(s) = \ln \ln s^{-1}$. We compute $\frac{1}{L(t_i)}$ at each time t_i, and also we check the following approximation parameter

$$\rho_i = \frac{L(t_i)}{L(t_{i+1})} \Big/ \ln \left(\frac{F_{i+1}/(T-t_{i+1})}{F_i/(T-t_i)} \right), \quad \text{where} \quad F_i = F(T-t_i). \tag{58}$$

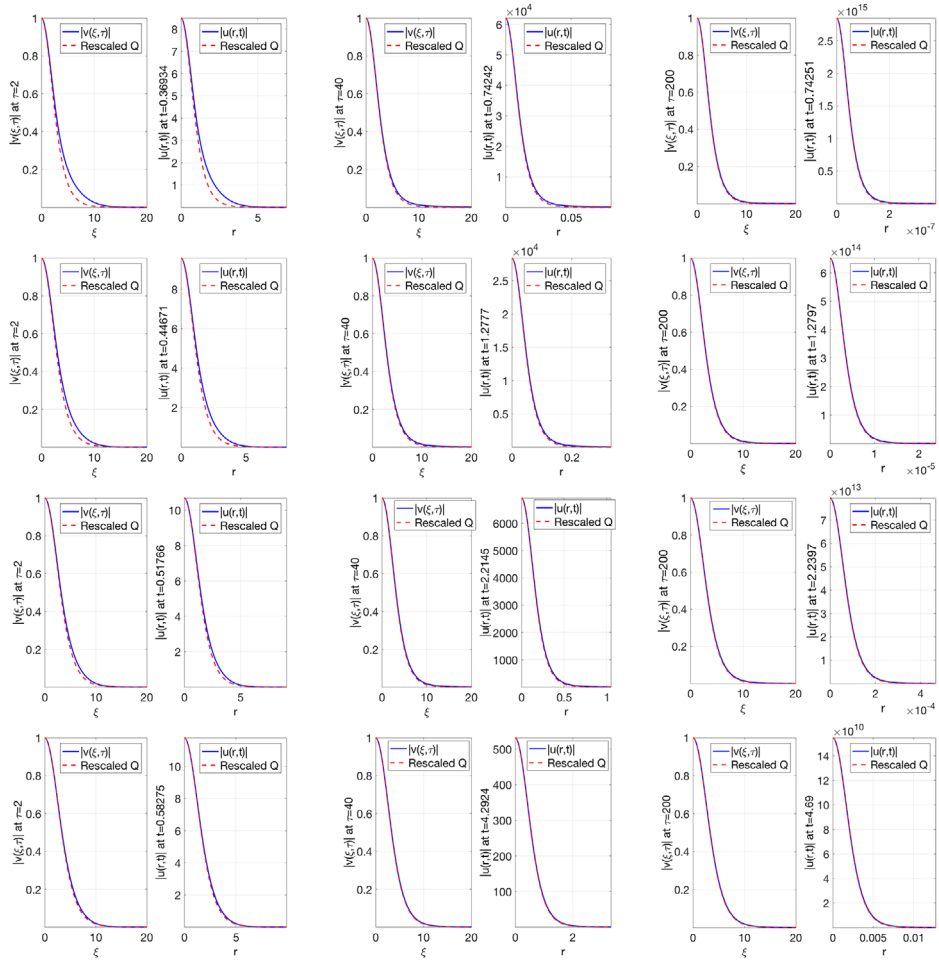

FIGURE 6 Convergence of blow-up profile in $d = 4$ (top), $d = 5$ (middle top), $d = 6$ (middle bottom), and $d = 7$ (bottom). We plot next to each other the rescaled profile $|v|$ in the rescaled time τ and the original solution $|u|$ in the actual time t. As $\tau \to \infty$ (here, $\tau = 2, 40, 200$), the profile (blue dots) approaches the rescaled ground state Q ($Q_{\text{rescaled}} = \frac{1}{L^{\alpha}(t)} Q(\frac{r}{L(t)})$)

Due to the leading square root decay, ρ is expected to be $\frac{1}{2}$, and thus, we check how fast the parameter ρ_i converges to $\frac{1}{2}$ and which choice of $F(s)$ gives the best approximation. In Refs. 22, 38 it was shown that $F(s) = \ln \ln s^{-1}$ provides the fastest convergence to $\frac{1}{2}$ as well as the best parameter ρ_i stabilization. Furthermore, $F(s) = \ln \ln s^{-1}$ gave the optimal quantity in the standard deviation ϵ: for computational purposes we define it on each subinterval of values of $1/L(t)$ (denoting by I_j the range of values, see, for example, Table 4)

$$\epsilon = \left(\frac{1}{\#|I_i|} \sum_{j \in I_i} \left(\frac{1}{2} - \rho_j \right)^2 \right)^{\frac{1}{2}}. \tag{59}$$

TABLE 4 3D case

The fitting power ρ_i from different corrections								
i	$\frac{1}{L(t)}$ range	$F(s)=1$	$F(s)=\ln\frac{1}{s}$	$F(s)=(\ln\frac{1}{s})^{0.5}$	$F(s)=(\ln\frac{1}{s})^{1/4}$	$F(s)=\ln\ln\frac{1}{s}$	$\gamma^\star$	F_{mal}
0	5e8 ∼ 4e9	0.5028	0.4908	0.4967	0.4997	0.4995	0.2291	0.5007
1	4e9 ∼ 3e10	0.5024	0.4916	0.4969	0.4997	0.4995	0.2198	0.5006
2	3e10 ∼ 3e11	0.5021	0.4922	0.4971	0.4996	0.4996	0.2120	0.5006
3	3e11 ∼ 2e12	0.5019	0.4927	0.4973	0.4996	0.4996	0.2055	0.5004
4	2e12 ∼ 2e13	0.5017	0.4932	0.4974	0.4996	0.4996	0.1998	0.5003
5	2e13 ∼ 1e15	0.5016	0.4936	0.4975	0.4996	0.4996	0.1948	0.5004
6	1e15 ∼ 7e15	0.5014	0.4939	0.4977	0.4995	0.4996	0.1904	0.5004
7	7e15 ∼ 5e16	0.5013	0.4942	0.4978	0.4995	0.4997	0.1865	0.5003
The ϵ_i from different corrections								
i	$\frac{1}{L(t)}$ range	$F(s)=1$	$F(s)=\ln\frac{1}{s}$	$F(s)=(\ln\frac{1}{s})^{0.5}$	$F(s)=(\ln\frac{1}{s})^{1/4}$	$F(s)=\ln\ln\frac{1}{s}$	F_{mal}	
0	5e8 ∼ 4e9	0.0028	0.0092	0.0033	2.53e-4	4.87e-4	7.12e-4	
1	4e9 ∼ 3e10	0.0026	0.0088	0.0032	2.95e-4	4.77e-4	6.70e-4	
2	3e10 ∼ 3e11	0.0025	0.0085	0.0031	3.27e-4	4.67e-4	6.46e-4	
3	3e11 ∼ 2e12	0.0023	0.0082	0.0030	3.50e-4	4.57e-4	5.98e-4	
4	2e12 ∼ 2e13	0.0022	0.0079	0.0029	3.67e-4	4.47e-4	5.56e-4	
5	2e13 ∼ 1e15	0.0021	0.0077	0.0028	3.83e-4	4.37e-4	5.32e-4	
6	1e15 ∼ 7e15	0.0021	0.0075	0.0028	3.93e-4	4.28e-4	5.14e-4	
7	7e15 ∼ 5e16	0.0020	0.0073	0.0027	4.01e-4	4.19e-4	4.91e-4	

Note. Top table: comparison of curve fitting for various choices of correction terms $F(s)$. Here, "$\frac{1}{L(t)}$ range" means values are in the range $\frac{1}{L(t_i)} \sim \frac{1}{L(t_{i+1})}$. Bottom table: standard deviation ϵ_i for different corrections $F(s)$ from the top table. The *log-log* correction produces the minimal error in ϵ_i.

We provide the results from our computations for the best fitting ρ_i and standard deviation ϵ_i in Tables 4-8 for dimensions $d = 3, \dots, 7$. One can notice that the *log-log* correction does the best minimization of the error in the fitting. We also find the optimal value of γ, denoted by $\gamma^\star$, such that $F(s) = (\ln s^{-1})^{\gamma^\star}$ gives the rate ρ_i to be exactly $\frac{1}{2}$. The parameter $\gamma^\star$ was introduced in Ref. 38, we also used it in Refs. 22 and found that even this parameter is decreasing, which also indicates that the correction should be weaker than $(\ln s^{-1})^\gamma$ for any γ. To compute $\gamma^\star$, we directly calculate ρ_i from (58), which gives

$$\frac{1}{\rho_i(\gamma)} = \frac{\gamma}{\rho_i(1)} + \frac{1-\gamma}{\rho_i(0)}, \tag{60}$$

together with

$$\rho_i(\gamma) = \frac{1}{2}. \tag{61}$$

Then we obtain the optimal $\gamma^\star$. Observe that the $\gamma^\star$ is decreasing as the magnitude of the range I_i is increasing, this is similar to the behavior and results in the L^2-critical NLS equation.

Some of the results are recorded in Tables 4-8, where we tested $F(s) = 1$, $F(s) = (\ln s^{-1})^\gamma$, $\gamma = 1, 0.5, 0.25$, and $F(s) = \ln\ln s^{-1}$; we also list the values of the optimal $\gamma^\star$ at the increasing

TABLE 5 4D case

The fitting power ρ_i from different corrections								
i	$\frac{1}{L(t)}$ range	$F(s)=1$	$F(s)=\ln\frac{1}{s}$	$F(s)=(\ln\frac{1}{s})^{0.5}$	$F(s)=(\ln\frac{1}{s})^{1/4}$	$F(s)=\ln\ln\frac{1}{s}$	$\gamma^\star$	F_{mal}
0	4e8 ∼ 3e9	0.5029	0.4906	0.4966	0.4997	0.4995	0.2281	0.5005
1	3e9 ∼ 3e10	0.5025	0.4913	0.4968	0.4996	0.4995	0.2179	0.5000
2	3e10 ∼ 2e11	0.5022	0.4920	0.4970	0.4996	0.4995	0.2095	0.5013
3	2e11 ∼ 2e12	0.5019	0.4925	0.4972	0.4995	0.4995	0.2024	0.4997
4	2e12 ∼ 1e13	0.5017	0.4930	0.4973	0.4995	0.4995	0.1963	0.5008
5	1e13 ∼ 1e14	0.5016	0.4934	0.4975	0.4995	0.4996	0.1910	0.5004
6	1e14 ∼ 7e14	0.5014	0.4938	0.4976	0.4995	0.4996	0.1863	0.5000
7	7e14 ∼ 5e15	0.5013	0.4941	0.4977	0.4995	0.4996	0.1821	0.5005
The ϵ_i from different corrections								
i	$\frac{1}{L(t)}$ range	$F(s)=1$	$F(s)=\ln\frac{1}{s}$	$F(s)=(\ln\frac{1}{s})^{0.5}$	$F(s)=(\ln\frac{1}{s})^{1/4}$	$F(s)=\ln\ln\frac{1}{s}$	F_{mal}	
0	2e7 ∼ 4e8	0.0050	0.0125	0.0039	6.55e-4	5.00e-4	4.79e-4	
1	4e8 ∼ 7e9	0.0046	0.0118	0.0038	5.86e-4	5.09e-4	3.38e-4	
2	7e9 ∼ 1e11	0.0042	0.0112	0.0037	5.53e-4	5.09e-4	7.87e-4	
3	1e11 ∼ 2e12	0.0039	0.0107	0.0035	5.36e-4	5.04e-4	6.99e-4	
4	2e12 ∼ 2e13	0.0037	0.0102	0.0034	5.28e-4	4.97e-4	7.16e-4	
5	2e13 ∼ 3e14	0.0035	0.0098	0.0033	5.23e-4	4.88e-4	6.72e-4	
6	3e14 ∼ 5e15	0.0033	0.0095	0.0032	5.20e-4	4.79e-4	6.22e-4	
7	5e15 ∼ 7e16	0.0032	0.0092	0.0031	5.17e-4	4.70e-4	6.04e-4	

Note. Top table: comparison of curve fitting for different choices of correction terms $F(s)$. Bottom table: the standard deviation ϵ_i for different corrections $F(s)$ from the above table. Similar to the 3D case, the *log-log* correction produces the minimal error in ϵ_i.

magnitude range. As we mentioned above, the $\gamma^\star$ decreases as the magnitude increases (and as the solution approaches the blow-up time T). This indicates that none of $(\ln s^{-1})^\gamma$ corrections are good choice. Therefore, a weaker correction than $(\ln s^{-1})^\gamma$ is needed, giving more support to the *log-log* correction. Besides the forms of the functional fitting corrections already discussed, we also include the results F_{mal} for the "Malkin adiabatic" law $L(t) \approx (2\sqrt{b}(T-t))^{1/2}$ for a comparison (details about the adiabatic laws are in Subsection 4.4).

4.3 | Second attempt: asymptotic analysis for the correction term

We follow the argument for the L^2-critical NLS equation in (Ref. 21, chapter 8). From asymptotic considerations we will confirm the hypothesis that $a(\tau) \sim 1/(\ln(\tau) + 3\ln\ln\tau)$, which leads to the *log-log* correction term on the blow-up rate for the L^2-critical gHartree equation, that is, we show that

$$L(t) \approx \left(\frac{2\pi(T-t)}{\ln\ln(\frac{1}{T-t})}\right)^{\frac{1}{2}}. \tag{62}$$

We note that while numerically we saw no difference in the blow-up regime for different dimensions, results in this section are conditional for dimensions $d \geq 5$, since the local well-posedness is not yet available in gHartree when $p < 2$ (or $\sigma < \frac{1}{2}$).

TABLE 6 5D case

The fitting power ρ_i from different corrections								
i	$\frac{1}{L(t)}$ range	$F(s)=1$	$F(s)=\ln\frac{1}{s}$	$F(s)=(\ln\frac{1}{s})^{0.5}$	$F(s)=(\ln\frac{1}{s})^{1/4}$	$F(s)=\ln\ln\frac{1}{s}$	$\gamma^\star$	F_{mal}
0	1e10 ∼ 4e10	0.5037	0.4931	0.4983	0.5010	0.5009	0.3453	0.5018
1	4e10 ∼ 2e11	0.5034	0.4934	0.4983	0.5009	0.5008	0.3359	0.5018
2	2e11 ∼ 7e11	0.5032	0.4936	0.4983	0.5007	0.5007	0.3275	0.5013
3	7e11 ∼ 3e12	0.5029	0.4939	0.4984	0.5006	0.5006	0.3198	0.5014
4	3e12 ∼ 1e13	0.5027	0.4941	0.4984	0.5005	0.5006	0.3066	0.5013
5	1e13 ∼ 5e13	0.5025	0.4943	0.4984	0.5005	0.5005	0.3009	0.5012
6	5e13 ∼ 2e14	0.5024	0.4945	0.4984	0.5004	0.5005	0.2956	0.5015
7	2e14 ∼ 7e14	0.5023	0.4947	0.4985	0.5003	0.5004	0.2906	0.5018

The ϵ_i from different corrections							
i	$\frac{1}{L(t)}$ range	$F(s)=1$	$F(s)=\ln\frac{1}{s}$	$F(s)=(\ln\frac{1}{s})^{0.5}$	$F(s)=(\ln\frac{1}{s})^{1/4}$	$F(s)=\ln\ln\frac{1}{s}$	F_{mal}
0	1e10 ∼ 4e10	0.0037	0.0069	0.0017	0.0010	9.09e-4	0.0018
1	4e10 ∼ 2e11	0.0036	0.0068	0.0017	9.54e-4	8.57e-4	0.0017
2	2e11 ∼ 7e11	0.0035	0.0065	0.0017	8.89e-4	8.11e-4	0.0016
3	7e11 ∼ 3e12	0.0033	0.0064	0.0017	8.33e-4	7.71e-4	0.0016
4	3e12 ∼ 1e13	0.0032	0.0063	0.0016	7.84e-4	7.36e-4	0.0015
5	1e13 ∼ 5e13	0.0031	0.0062	0.0016	7.41e-4	7.04e-4	0.0015
6	5e13 ∼ 2e14	0.0030	0.0061	0.0016	7.03e-4	6.76e-4	0.0015
7	2e14 ∼ 7e14	0.0029	0.0060	0.0016	56.69e-4	6.50e-4	0.0015

Note. Top table: comparison of curve fitting for various choices of $F(s)$. Bottom table: standard deviation ϵ_i for different $F(s)$ from the above table. As in 3D, 4D, the *log-log* correction produces the minimal error in ϵ_i.

4.3.1 | Slow decay of $a(\tau)$

Recalling the proof of Proposition 3, we note that the blow-up solutions have the quadratic phase

$$\theta(\xi) = -a\xi^2/4. \tag{63}$$

Writing $Q = e^{-ia\xi^2/4}P$, we have P satisfy

$$\begin{cases} \Delta P - P + \frac{a^2\xi^2}{4}P - ia\frac{d\sigma-2}{2\sigma}P + \left((-\Delta)^{-1}|P|^{2\sigma+1}\right)|P|^{2\sigma-1}P = 0, \\ P_\xi(0) = 0, \quad P(\xi) = 0 \quad \text{as} \quad \xi \to \infty, \quad P(0) \quad \text{is real.} \end{cases} \tag{64}$$

Note that when $a = 0$, (64) reduces to the (L^2-critical) ground state (to distinguish it here, we write R instead of Q):

$$\Delta R - R + \left((-\Delta)^{-1}|R|^{2\sigma+1}\right)|R|^{2\sigma-1}R = 0. \tag{65}$$

This suggests that the blow-up profiles converge to the ground state R as $a \to 0$, which matches our numerical observations shown in Figures 5 and 6. The following proposition shows that $a(\tau)$ decays to zero slower than any polynomial rate. For that we vary the dimension d, which is possible, as in the radial setting it only appears as the coefficient, and thus, we can define a continuous

TABLE 7 6D case

The fitting power ρ_i from different corrections								
i	$\frac{1}{L(t)}$ range	$F(s)=1$	$F(s)=\ln\frac{1}{s}$	$F(s)=(\ln\frac{1}{s})^{0.5}$	$F(s)=(\ln\frac{1}{s})^{0.25}$	$F(s)=\ln\ln\frac{1}{s}$	$\gamma^\star$	F_{mal}
0	1e10 ∼ 4e10	0.5036	0.4929	0.4982	0.5009	0.5008	0.3322	0.5028
1	4e10 ∼ 2e11	0.5033	0.4932	0.4982	0.5008	0.5007	0.3250	0.5044
2	2e11 ∼ 7e11	0.5031	0.4935	0.4983	0.5007	0.5006	0.3184	0.4951
3	7e11 ∼ 3e12	0.5029	0.4938	0.4983	0.5006	0.5006	0.3124	0.5084
4	3e12 ∼ 1e13	0.5027	0.4940	0.4983	0.5005	0.5005	0.3069	0.4972
5	1e13 ∼ 4e13	0.5025	0.4942	0.4983	0.5004	0.5005	0.3018	0.5013
6	4e13 ∼ 1e14	0.5024	0.4946	0.4984	0.5004	0.5004	0.2970	0.5046
7	1e14 ∼ 5e14	0.5023	0.4948	0.4984	0.5003	0.5004	0.2926	0.4981

The ϵ_i from different corrections							
i	$\frac{1}{L(t)}$ range	$F(s)=1$	$F(s)=\ln\frac{1}{s}$	$F(s)=(\ln\frac{1}{s})^{0.5}$	$F(s)=(\ln\frac{1}{s})^{0.25}$	$F(s)=\ln\ln\frac{1}{s}$	F_{mal}
0	1e10 ∼ 4e10	0.0036	0.0071	0.0018	9.16e-4	7.68e-4	0.0028
1	4e10 ∼ 2e11	0.0035	0.0069	0.0018	8.89e-4	7.30e-4	0.0037
2	2e11 ∼ 7e11	0.0034	0.0068	0.0018	8.29e-4	6.97e-4	0.0041
3	7e11 ∼ 3e12	0.0032	0.0067	0.0018	7.78e-4	6.67e-4	0.0055
4	3e12 ∼ 1e13	0.0031	0.0065	0.0017	7.32e-4	6.41e-4	0.0051
5	1e13 ∼ 4e13	0.0030	0.0064	0.0017	6.92e-4	6.16e-4	0.0047
6	4e13 ∼ 1e14	0.0030	0.0063	0.0017	6.56e-4	5.94e-4	0.0046
7	1e14 ∼ 7e14	0.0029	0.0062	0.0017	6.24e-4	5.74e-4	0.0045

Note. Top table: comparison of the curve fitting for different choices of $F(s)$. Bottom table: standard deviation ϵ_i for different $F(s)$ from the above table. The *log-log* correction produces the minimal error in ϵ_i.

function $d = d(a)$, for a fixed nonlinearity σ, and depending on the parameter a. We show later (similar to the NLS case in Ref. 21, section 8.1.4), the diminishing criticality $s_c \to 0$, or dimension $d \to \frac{2}{\sigma}$, which involves the complex term in (64) with

$$\nu(a) \stackrel{\text{def}}{=} ia\,\frac{\sigma d - 2}{2\sigma} \longrightarrow 0, \tag{66}$$

is responsible for the *log-log* correction in the blow-up rate.

Proposition 4. *If Q is a solution of (16) with finite Hamiltonian, the function $d(a)$ is differentiable to all orders at $a = 0$ and*

$$\frac{d^p}{da^p}\left(d(a) - \frac{2}{\sigma}\right)|_{a=0} = 0 \quad \textit{for} \quad \textit{all} \quad p = 0, 1, 2, \dots . \tag{67}$$

The proof for Proposition 4 is similar to the one of Proposition 8.1 in (Ref. 21, chapter 8) with the appropriate modifications of the identities involving the potential term, and the fact that the nonzero constant Hamiltonian of Q gives the same conclusion as the zero Hamiltonian of Q in the NLS case. We only show the differences.

TABLE 8 7D case

The fitting power ρ_i from different corrections								
i	$\frac{1}{L(t)}$ range	$F(s)=1$	$F(s)=\ln\frac{1}{s}$	$F(s)=(\ln\frac{1}{s})^{0.5}$	$F(s)=(\ln\frac{1}{s})^{1/4}$	$F(s)=\ln\ln\frac{1}{s}$	$\gamma^\star$	F_{mal}
0	6e9 ∼ 4e10	0.5033	0.4924	0.4978	0.5005	0.5004	0.2983	0.5127
1	4e10 ∼ 2e11	0.5030	0.4929	0.4979	0.5004	0.5004	0.2930	0.4924
2	2e11 ∼ 1e12	0.5028	0.4932	0.4980	0.5004	0.5003	0.2880	0.4432
3	1e12 ∼ 8e12	0.5025	0.4937	0.4981	0.5003	0.5003	0.2834	0.3996
4	8e12 ∼ 4e13	0.5024	0.4940	0.4981	0.5002	0.5003	0.2792	0.6070
5	4e13 ∼ 2e14	0.5022	0.4943	0.4982	0.5002	0.5003	0.2752	0.5287
6	2e14 ∼ 1e15	0.5021	0.4946	0.4983	0.5002	0.5002	0.2715	0.5070
7	1e15 ∼ 7e15	0.5019	0.4948	0.4983	0.5001	0.5002	0.2680	0.4918

The ϵ_i from different corrections							
i	$\frac{1}{L(t)}$ range	$F(s)=1$	$F(s)=\ln\frac{1}{s}$	$F(s)=(\ln\frac{1}{s})^{0.5}$	$F(s)=(\ln\frac{1}{s})^{1/4}$	$F(s)=\ln\ln\frac{1}{s}$	F_{mal}
0	6e9 ∼ 4e10	0.0033	0.0076	0.0022	5.32e-4	3.94e-4	0.0127
1	4e10 ∼ 2e11	0.0032	0.0074	0.0022	4.88e-4	3.79e-4	0.0105
2	2e11 ∼ 1e12	0.0030	0.0071	0.0021	4.50e-4	3.65e-4	0.0339
3	1e12 ∼ 8e12	0.0029	0.0070	0.0021	4.17e-4	3.52e-4	0.1035
4	8e12 ∼ 4e13	0.0028	0.0068	0.0020	3.89e-4	3.40e-4	0.1042
5	4e13 ∼ 2e14	0.0027	0.0066	0.0020	3.65e-4	3.29e-4	0.0959
6	2e14 ∼ 1e15	0.0026	0.0065	0.0020	3.43e-4	3.18e-4	0.0888
7	1e15 ∼ 7e15	0.0026	0.0063	0.0019	3.24e-4	3.09e-4	0.0831

Note. Top table: comparison of curve fitting for different choices of $F(s)$. Bottom table: standard deviation ϵ_i for different $F(s)$ from the above table. The *log-log* correction produces the minimal error in ϵ_i.

Lemma 3. *For R in (65), we have*

$$\int \left(|R_\xi|^2 - \frac{1}{2\sigma+1} V(R) \right) \xi^{d-1} d\xi = 0. \tag{68}$$

For ρ satisfying

$$\Delta\rho - \rho + 2\sigma\big((-\Delta)^{-1}R^{2\sigma+1}\big)R^{2\sigma-1}\rho + (2\sigma+1)\big((-\Delta)^{-1}R^{2\sigma}\rho\big)R^{2\sigma} = -\frac{1}{4}\xi^2 R, \tag{69}$$

we have

$$\int \left(R\rho - \frac{1}{8}\xi^2 R^2 \right) \xi^{d-1} d\xi = 0. \tag{70}$$

For g solving

$$\Delta g - g + 2\sigma\big((-\Delta)^{-1}R^{2\sigma+1}\big)R^{2\sigma-1}g + (2\sigma+1)\big((-\Delta)^{-1}R^{2\sigma}g\big)R^{2\sigma} = -\xi^{-1}R_\xi, \tag{71}$$

we have

$$-2\int Rg\xi^{d-1}d\xi + \int \left(R_\xi^2 - \frac{1}{2\sigma+1}V(R) \right) \xi^{d-1}\ln\xi d\xi = \frac{1}{2}\int R^2\xi^{d-1}d\xi. \tag{72}$$

Proof. The identity (68) is simply the Pohozaev identity. To get (70), we consider

$$\Delta P - P + \frac{a^2\xi^2}{4}P + V(P) = 0, \tag{73}$$

which is the perturbation of the ground state equation (65). When $s_c = 0$ (critical case), let

$$P^{(n)} = R + \frac{a^2}{2}P_2 + \cdots + \frac{a^{2n}}{(2n)!}P_n \tag{74}$$

be a sequence of approximations of (73) with monotonic profiles $P^{(n)}$ that obey

$$\Delta P^{(n)} - P^{(n)} + \frac{a^2\xi^2}{4}P^{(n)} + V(P^{(n)}) = O(a^{2n+2}). \tag{75}$$

For a fixed a, $P(0;a) \equiv P(0)$ is real, so is $P^{(n)}(0;a)$, and consequently, $P^{(n)}(\xi;a)$ is real for any n. The estimate for the Hamiltonian of $P^{(n)}$ is

$$H(P^{(n)}) = \int \left(|P^{(n)}_\xi|^2 - \frac{1}{2\sigma+1}V(P^{(n)}) + \frac{a^2\xi^2}{4}|P^{(n)}|^2 \right)\xi^{d-1}d\xi = O(a^{2n+2}). \tag{76}$$

Putting (74) in (76), the coefficients of $P^{(2)}$ produce the identity (70).

To prove (72), we first obtain the following list of identities:

$$-2\sigma \int g\big((-\Delta)^{-1}R^{2\sigma+1}\big)R^{2\sigma}\xi^{d-1}d\xi = \int R\frac{R_\xi}{\xi}\xi^{d-1}d\xi\,, \tag{77}$$

$$-2\int g\Delta R\xi^{d-1}d\xi = \int R^2_\xi\xi^{d-1}d\xi\,, \tag{78}$$

$$-\int \Big(R^2_\xi + R^2 - V(R)\Big)\ln\xi\,\xi^{d-1}d\xi = \int R\frac{R_\xi}{\xi}\xi^{d-1}d\xi\,, \tag{79}$$

$$\int \left((1-\sigma)R^2_\xi + R^2 - \frac{1}{2\sigma+1}V(R)\right)\ln\xi\,\xi^{d-1}d\xi = (1-\sigma/2)\int R^2\xi^{d-1}d\xi. \tag{80}$$

The proof of the above four identities comes from Pohozaev identities and is similar to the proof in (Ref. 21, chapter 8, Lemma 8.3), replacing $R^{2\sigma+1}$ with $((-\Delta)^{-1}R^{2\sigma+1})R^{2\sigma}$ and such. ∎

Proof of Proposition 4. We again follow (Ref. 21, chapter 8, Proposition 8.1) using Lemma 3 and recalling (31). We only note the modifications needed in this case, the rest follows the NLS case. Considering $d = d(a)$ as a function of a, differentiating (31) with respect to a, and evaluating at $a = 0$ ($d(0) = 2/\sigma$) gives

$$\int \left(-\Delta R - \big((-\Delta)^{-1}R^{2\sigma+1}\big)R^{2\sigma}\right)\mathrm{Re}(p_1)\xi^{d-1}d\xi + d'(0)\int \left(R^2_\xi - \frac{1}{2\sigma+1}V(R)\right)\ln\xi\,\xi^{d-1}d\xi = 0, \tag{81}$$

where $p_1 = \frac{dP}{da}|_{a=0}$ solves

$$\Delta p_1 - p_1 + 2\sigma\big((-\Delta)^{-1}R^{2\sigma+1}\big)R^{2\sigma-1}p_1 + (2\sigma+1)\big((-\Delta)^{-1}R^{2\sigma}p_1\big)R^{2\sigma} = -d'(0)\frac{R_\xi}{\xi}.$$

For the rest of the proof, replace the term $R^{2\sigma+1}$ with $((-\Delta)^{-1}R^{2\sigma+1})\,R^{2\sigma}$, then the term $R^{2\sigma+2}$ with $((-\Delta)^{-1}R^{2\sigma+1})R^{2\sigma+1}$ and the linearized term $(2\sigma+1)R^{2\sigma}g$ with $2\sigma((-\Delta)^{-1}R^{2\sigma+1})R^{2\sigma-1}g$ $+(2\sigma+1)((-\Delta)^{-1}R^{2\sigma}g)R^{2\sigma}$. ■

4.3.2 | Convergence of profiles as $a \to 0$, or a nonuniform limit

We are now ready to conclude the convergence of profiles Q in the slightly L^2-supercritical case to the profiles R of the L^2-critical case as $a \to 0$, recalling that the ground state H^1 solutions R have zero Hamiltonian and could be obtained via minimization as described in Ref. 12, in particular, the value $\|R\|_{L^2}$ is uniquely defined. The proof of the following statement is verbatum (with modifications in the potential term as above) of (Ref. 21, Proposition 8.4)

Proposition 5. *When $a \to 0^+$, and hence, $d(a) \searrow d(0) = \frac{2}{\sigma}$, admissible solutions Q of (16) satisfy*

i. for $a\xi \ll 1$, $Q \approx R(\xi)e^{-ia\xi^2/4}$; equivalently, the solution P of (64) approaches the ground state R;
ii. for $a\xi \gg 1$, $Q \approx \mu\,\xi^{-\frac{1}{\sigma}-\frac{i}{a}}$ with $\mu^2 = d - \frac{2}{\sigma}\|R\|_{L^2}^2$;
iii. the asymptotic behavior of $d(a)$, or correspondingly, $\nu(a) = a(\frac{d}{2} - \frac{1}{\sigma})$, is given by

$$d(a) \approx \frac{2}{\sigma} + \frac{2\,\nu_0^2}{a\|R\|_{L^2}^2}\,e^{-\pi/a}, \quad \text{or} \quad \nu(a) \approx \frac{\nu_0^2}{\|R\|_{L^2}^2}e^{-\pi/a}, \quad \text{with} \quad \nu_0 = \lim_{\xi\to\infty}\xi^{\frac{d-1}{2}}e^{\xi}R(\xi). \tag{82}$$

Finally, we describe the construction of the *log-log* blow-up solutions.

4.3.3 | Construction of asymptotic solutions

We return to Equation (13) and follow the argument in (Ref. 21, chapter 8.2). The change of variables with the quadratic phase $v = e^{i\tau - ia\xi^2/4}w$ gives

$$iw_\tau + \Delta w - w + \frac{1}{4}b(\tau)\xi^2 w + \big((-\Delta)^{-1}|w|^{2\sigma+1}\big)|w|^{2\sigma-1}w = 0, \tag{83}$$

where

$$b(\tau) = a^2 + a_\tau = -L^3L_{tt}, \tag{84}$$

with the parameter L defined in Section 2 ($a = -LL_t$). We would like to obtain explicit dependence of b on τ as $\tau \to \infty$. Writing

$$w(\xi,\tau) = P(\xi, b(\tau)) + W(\xi,\tau) \quad \text{with} \quad W \ll P,$$

we have P solve

$$\begin{cases} \Delta P - P + \frac{b\xi^2}{4} P - i\nu(\sqrt{b})P + \left((-\Delta)^{-1}|P|^{2\sigma+1}\right)|P|^{2\sigma-1}P = 0, \\ P_\xi(0) = 0, \quad P(0) \quad \text{is real}, \quad P(\xi) = 0 \quad \text{as} \quad \xi \to \infty, \end{cases} \tag{85}$$

and also satisfy the *finite* Hamiltonian condition

$$\int_{\mathbb{R}^d} \left(|P_\xi|^2 - \frac{1}{2(2\sigma+1)}\left((-\Delta)^{-1}|P|^{2\sigma+1}\right)|P|^{2\sigma+1} + \sqrt{b}\,\mathrm{Im}\left(\xi P \bar{P}_\xi\right) + \frac{b}{4}\xi^2|P|^2 \right) d\xi = const. \tag{86}$$

Considering a_τ to be of the lower order than a^2 in (84) (similar to the NLS), we have $a \approx \sqrt{b}$ (which is also confirmed later), and therefore, the parameter ν in (85) is approximated for large times τ as

$$\nu(\sqrt{b}) \approx \frac{\nu_0^2}{\|R\|_{L^2}^2} e^{-\pi/\sqrt{b}}. \tag{87}$$

The following proposition determines b as a function of τ from the condition that the decomposition $w(\xi,\tau) = P(\xi, b(\tau)) + W(\xi,\tau)$ is an asymptotic solution of (83).

Proposition 6. *Collapsing solutions of the generalized Hartree equation in the critical case* $p = \frac{4}{d} + 1$, *or equivalently* $\sigma = 2/d$, *near a singularity have the asymptotic form*

$$u(x,t) \approx \frac{1}{L(t)} e^{i(\tau(t) - a(t)\frac{|x|^2}{4L^2(t)})} P\left(\frac{|x|}{L(t)}, b(t)\right), \tag{88}$$

where

$$\tau_t = L^{-2}, \qquad -LL_t = a, \qquad L^3 L_{tt} = -b, \tag{89}$$

and $b = a^2 + a_\tau \approx a^2$ *obeys*

$$b_\tau = -\frac{2\|R\|_{L^2}^2}{M}\,\nu(\sqrt{b}) \approx -\frac{2\nu_0^2}{M} e^{-\pi/\sqrt{b}}, \tag{90}$$

where $M = \frac{1}{4}\int_{\mathbb{R}^d} R^2\xi^2 d\xi$ *is the momentum.*

The proof of this proposition is verbatim adapted from (Ref. 21, Proposition 8.5) as the only difference is in the nonlinear term, which plays no role in the analysis here.

We state the next two propositions about the *log-log* law and its range, omitting the proofs as the nonlinearity no longer affects them.

Proposition 7. *The leading order in the expansion for $a(\tau)$ as $\tau \to \infty$ is*

$$a(\tau) \approx b^{1/2} \approx \frac{\pi}{\ln \tau}. \tag{91}$$

The corresponding scaling factor $L(t)$ has the asymptotic form

$$L(t) \approx \left(\frac{2\pi(T-t)}{\ln \ln \frac{1}{T-t}} \right)^{1/2}. \tag{92}$$

In addition,

$$\tau(t) \approx \frac{1}{2\pi} \ln \left(\frac{1}{T-t} \right) \ln \ln \left(\frac{1}{T-t} \right). \tag{93}$$

Proposition 8. *The asymptotic form of the solution given in Proposition 3.5 extends in the range $0 < r < r_{out}$, where*

$$r_{out} \approx 1/\sqrt{b} \sim \ln \ln \left(\frac{1}{T-t} \right). \tag{94}$$

4.4 | Adiabatic regime

From the asymptotic analysis in Subsection 4.3 and fitting analysis in Subsection 4.2, the blow-up rate follows the *log-log* regime at the *very high* focusing, which is currently impossible to observe numerically. The fittings in Subsection 4.2 indicate that there may be other laws for the blow-up rate before reaching the *log-log* level. In the NLS equation, the solution reaches the *adiabatic* regime, which can be numerically observed, before finally settling into the *log-log* regime. In this section, we show that the gHartree equation also has the *adiabatic* regime.

Recalling (89) and (90), we have

$$L_{tt} = -L^{-3} b, \qquad b_\tau = -\nu(\sqrt{b}) \quad \text{with} \quad \nu(\sqrt{b}) = -c_\nu e^{-\pi/\sqrt{b}}, \tag{95}$$

where c_ν is a positive constant. The equations in (95) are called the reduced equations in the L^2-critical NLS equation, see (Ref. 19, chapters 17 and 18). The NLS analysis gives, for example, two adiabatic laws:

$$L(t) = \sqrt{2\sqrt{b}(T-t)} \qquad \text{(Malkin Law)}, \tag{96}$$

and

$$L(t) \approx \sqrt{2\sqrt{b}(T-t) + C(t)(T-t)^2}, \quad C(t) = \frac{a^2 - b}{L^2} = -\frac{a_\tau}{L^2} \quad \text{(Fibich Law)}. \tag{97}$$

We next show how well the numerical solution matches these two adiabatic laws. The parameter $b = a^2 + a_\tau$ is obtained from calculating the value a_τ by the fourth-order backward difference

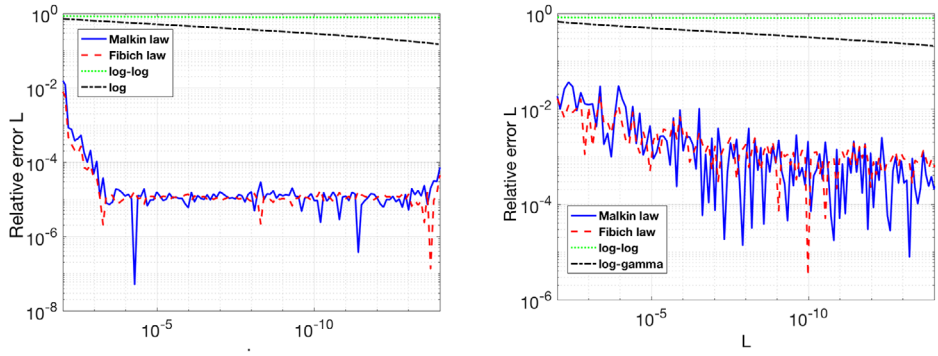

FIGURE 7 Consistency check: the relative error for two adiabatic laws compared to the *log-log* and γ-laws for the L^2-critical NLS equation in 2D and 4D. Left: 2D case with $u_0 = 2.77e^{-r^2}$, this plot is similar to the right plot in (Ref. 19, fig. 18.4)). Right: 4D case with $u_0 = 4e^{-r^2}$

(higher or lower order of finite difference method can also be applied but we found that they do not make much difference). Suppose that the rate $L(t)$ is the blow-up rate from the computational simulation, and $F(t)$ is the predicted rate (Malkin law or Fibich law). We show how the relative error

$$\mathcal{E}_r = \left| \frac{L(t)}{F(t)} - 1 \right| \tag{98}$$

changes as the time $t \to T$. For comparison, we also show the relative error for the *log-log* law and the γ-law with $\gamma = 1$, see Figure 8. As in the NLS, we take the constant equals to 2π in the γ-law, that is,

$$L(t) \approx \sqrt{\frac{T-t}{2\pi \ln \frac{1}{T-t}}}.$$

To test the consistency, we report the relative error for the 2D NLS equation case in Figure 7, which is similar to the plot in (Ref. 19, fig. 18.4), indicating that our numerical method is trustful. On the right subplot in Figure 7 we show the numerical error (also for the NLS) in the 4D case.

From Figure 8, we can see that adiabatic Malkin and Fibich laws are both equally good (except for the case $d = 3$, where Malkin law seems to be producing a slightly smaller error). Both Malkin law and Fibich law are better than the γ-law or the *log-log* law, this is due to the intermediate range of focusing (the *log-log* regime is yet to be reached at much higher focusing level). We only show the γ-law with $\gamma = 1$, since this option of γ is the best among other values in the adiabatic regime.

In dimensions $d = 3$ and $d = 4$, we note that there exist ranges of focusing regime that almost coincide in terms of the relative error, where the *log*-law (with $\gamma = 1$) is as good as the two adiabatic laws (for 3D the range $L \sim 10^{-6}$ and for 4D the range $L \sim 10^{-11}$). This supports our calculations that the adiabatic Malkin law (also possibly Fibich law) have the rates with the leading order $\ln \frac{1}{s}$ (i.e., $\gamma = 1$).

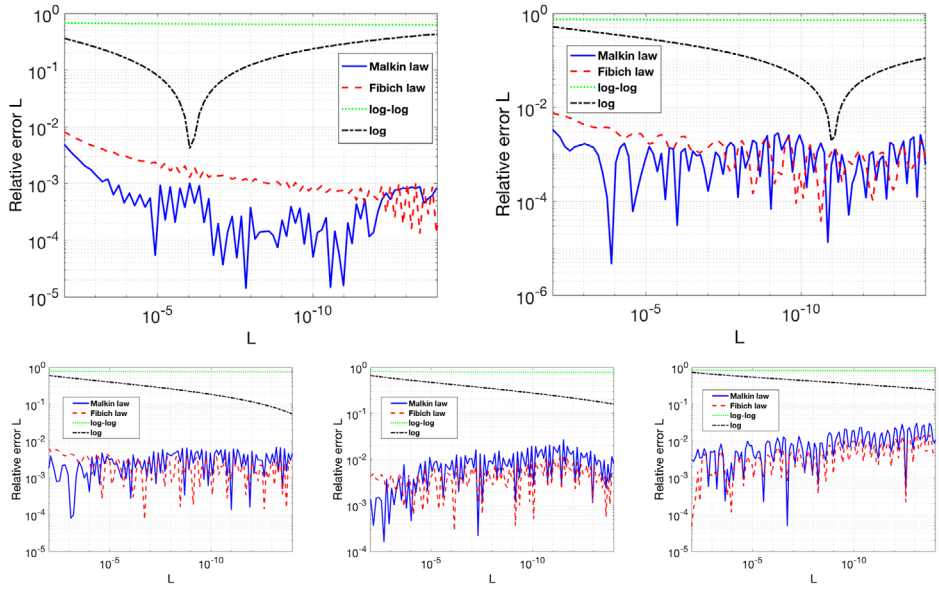

FIGURE 8 The relative error in gHartree case for different laws including adiabatic regimes, in dimensions $d = 3, 4, 5, 6, 7$

5 | THE L^2-SUPERCRITICAL CASE

In this section, we consider the blow-up dynamics in the L^2-supercritical gHartree equation. As the existence and *local uniqueness* theory of self-similar profile solutions was discussed in Section 2, we now introduce our numerical method for finding such blow-up profiles. Afterwards, we simulate the blow-up solutions for several L^2-supercritical gHartree equations and show the results of the convergence of the stable blow-up to the specific profiles and the rate.

5.1 | Numerical approach to compute profiles Q

We start with recalling that admissible solutions to the profile equation (16) are the ones without the fast oscillating decay in $Q = \alpha Q_1 + \beta Q_2$, where $Q_1 \approx |\xi|^{-\frac{i}{a}-\frac{1}{\sigma}}$, $Q_2 \approx e^{-\frac{ia\xi^2}{2}}|\xi|^{-\frac{i}{a}-d+\frac{1}{\sigma}}$ as $|\xi| \to \infty$, and thus, we are looking for the solutions with $\beta = 0$. Excluding Q_2, we note that the solution Q must be linearly dependent to Q_1 as $\xi \to \infty$, thus, computing the Wronskian for Q and Q_1 gives $(\frac{1}{\sigma} + \frac{i}{a})Q(\xi) + \xi\, Q_\xi(\xi) = 0$ as $\xi \to \infty$. This gives the artificial boundary condition

$$\left(\frac{1}{\sigma} + \frac{i}{a}\right)Q(K) + KQ_\xi(K) = 0 \tag{99}$$

by taking sufficiently large K.

We next split Q into the real and imaginary parts $Q = P + iW$, rewriting (16) and (99) as

$$\begin{cases} \Delta P - P - a(\frac{W}{\sigma} + \xi W_\xi) + ((-\Delta)^{-1}(P^2+W^2)^{\sigma+\frac{1}{2}})(P^2+W^2)^{\sigma-\frac{1}{2}}P = 0, \\ \Delta W - W + a(\frac{P}{\sigma} + \xi P_\xi) + ((-\Delta)^{-1}(P^2+W^2)^{\sigma+\frac{1}{2}})(P^2+W^2)^{\sigma-\frac{1}{2}}W = 0, \\ P_\xi(0) = 0, \\ W(0) = 0, \\ W_\xi(0) = 0, \\ \frac{1}{\sigma}P - \frac{1}{a}W + KP_\xi = 0, \\ \frac{1}{a}P + \frac{1}{\sigma}W + KW_\xi = 0. \end{cases} \tag{100}$$

We solve the equation system (100) in two ways. We first use the matlab solver *bvp4c*. We set $-\Delta\varphi = (P^2+W^2)^{\sigma+0.5}$ to deal with the nonlocal term. Thus, our solver will deal with a system of six equations. An alternative way to work with this system is to rewrite it into a system of nonlinear algebraic equations. Then the matlab solver *fsolve* can be applied (with the algorithm option *"levenberg-marquardt"* to make sure it converges).

During the computation, these two methods generate almost the same profiles. The residue shows that *fsolve* is more accurate if we use $N = 257$ Chebyshev-collocation points in our computations. Furthermore, both methods need a suitable initial guess. As we have previously handled NLS (see Ref. 22), we take the solution of the following NLS boundary value problem as our initial guess:

$$(NLS)_d \begin{cases} \Delta P - P - a(\frac{W}{\sigma} + \xi W_\xi) + (P^2+W^2)^{\sigma}P = 0, \\ \Delta W - W + a(\frac{P}{\sigma} + \xi P_\xi) + (P^2+W^2)^{\sigma}W = 0, \\ P_\xi(0) = 0, \\ W(0) = 0, \\ W_\xi(0) = 0, \\ \frac{1}{\sigma}P - \frac{1}{a}W + KP_\xi = 0, \\ \frac{1}{a}P + \frac{1}{\sigma}W + KW_\xi = 0. \end{cases} \tag{101}$$

In Ref. 23, we obtained solutions of this NLS system (101), hence, we can use them as our initial guess.

Similar to the NLS case, there are multiple solutions to the system (100), and we are able to find some of them, though not all these solutions are profiles for *stable* blow-up. Most likely they serve as profiles for the unstable blow-up solutions, but we have not verified that. In order to find the appropriate admissible profiles, constraints can be put either on the parameter a or on the value $Q(0)$. Here, we choose to put constraints on the parameter a, that is, we find the value of a such that $\alpha \le a \le \beta$ for prescribed constants α and β. In order to put these constraints into (100), we consider a mapping $f : \mathbb{R} \to [\alpha, \beta]$ and set

$$a(s) = \alpha f(s) + \beta(1 - f(s)),$$

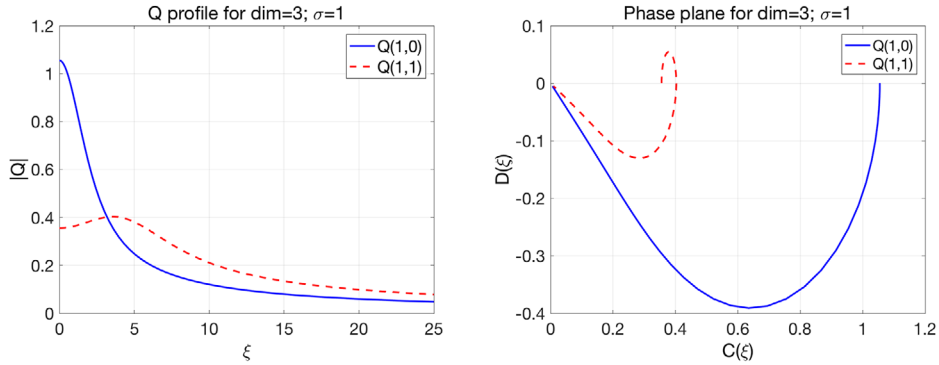

FIGURE 9 Q profiles for $d = 3, \sigma = 1$. Left: the monotone solution $Q_{1,0}$ (blue) and the first bifurcation solution $Q_{1,1}$ (red). Right: the phase plane (C, D), here $D \sim -C$

where $s \in \mathbb{R}$ and $f(s) \in [0, 1]$. Then, we solve Equation (100) by substituting $a(s) = \alpha f(s) + \beta(1 - f(s))$ with an explicitly given function $f(s)$. For example, one can take $a = \alpha \sin^2 s + \beta \cos^2 s$. The constant a is reconstructed after obtaining the value s.

We emphasize that while we are able to put the constraints into Equation (100), we still need a relatively suitable initial guess. This issue is similar to the NLS L^2-supercritical case: selecting initial guess to find the profiles with no oscialltions as $\xi \to \infty$ is extremely sensitive. For example, as discussed in Ref. 48, the initial guess is sensitive to 4% difference of the actual values of a and $Q(0)$ (to give convergence to the corresponding multi-bump profile). We choose the corresponding multi-bump solutions from NLS equation in Ref. 23, as the initial guess, which is suitable in the gHartree setting.

5.2 | Admissible profiles

Among all admissible solutions to (16) there is no uniqueness as it was shown in Refs. 23, 48, 53. These solutions generate branches of multi-bump profiles. We label the solution $Q_{1,0}$ the first solution in the branch $Q_{1,K}$ (this is the branch, which converges to the L^2-critical ground state solution R as $s_c \to 0$), and we consider $Q_{1,0}$ as the potential profile for stable gHartree blow-up, see the blue curve in Figure 9. By using another initial guess for parameters a and $Q(0)$ as described above, we obtain the solution $Q_{1,1}$, which is the first bifurcation from $Q_{1,0}$ (see the red dashed curve in Figure 9).

To better understand the dependence of solutions on parameters a and $Q(0)$, we study the pseudo-phase plane, which was introduced in the NLS case by Kopell and Landman in Ref. 53, and adopted in Budd, Chen and Russell.[48] We write

$$Q \equiv C(\xi) \exp\left(i \int_0^\xi \psi \right), \qquad D(\xi) = C_\xi / C \equiv \mathrm{Re}(Q_\xi / Q). \tag{102}$$

In other words, C is the amplitude of Q, $C(\xi) = |Q(\xi)|$, D is its logarithmic derivative, and ψ is the gradient of the phase. In the coordinates (C, D) we track the behavior of the graph as it decreases down to the origin when both C and D approach zero as $\xi \to \infty$. To see that recall from (28) that

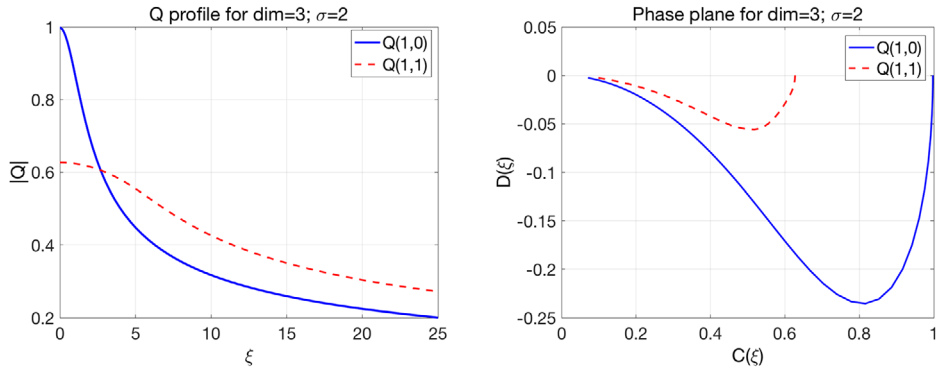

FIGURE 10 Q profile for $d = 3, \sigma = 2$. Left: the monotone solution $Q_{1,0}$ (blue) and the first bifurcation solution $Q_{1,1}$ (red). Right: the phase plane (C, D), here $D \sim -C^2$

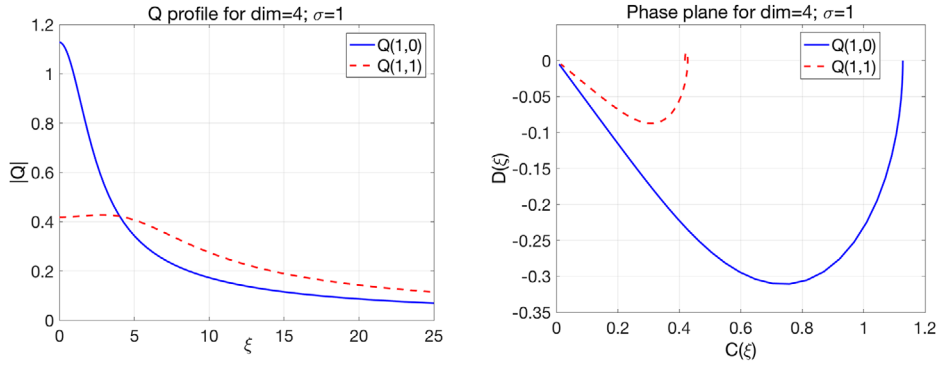

FIGURE 11 Q profile for $d = 4, \sigma = 1$. Left: the monotone solution $Q_{1,0}$ (blue) and the first bifurcation solution $Q_{1,1}$ (red). Right: the phase plane (C, D), here $D \sim -C$

asymptotically

$$Q(\xi) \sim \alpha\, \xi^{-\frac{1}{\sigma}} \exp\left(-\frac{i}{a}\, \log(\xi)\right) + \beta\, \xi^{-(d-\frac{1}{\sigma})} \exp\left(-\frac{i\, a\, \xi^2}{2} + \frac{i}{a} \log(\xi)\right),$$

where the first term is slowly decaying and the second term decays faster with rapid oscillations. The solution Q that varies slowly at infinity would have no oscillations at the end of the curve (as $C \to 0$), as

$$C \sim \frac{\alpha}{\xi^{1/\sigma}} \quad \text{and} \quad D \sim -\frac{1}{\sigma\, \xi} \quad \text{as} \quad \xi \to \infty.$$

Thus, such solutions will approach the origin in coordinates (C, D) along the curve $D \sim -\frac{1}{\sigma\, \alpha^\sigma}\, C^\sigma$. In the case of $\sigma = 1$, this will be a straight line with slope $-1/\alpha$, which we demonstrate in the paths shown in Figures 9 and 11 (right plot). In the case of $\sigma = 2$, this will be a parabola $D \sim -\frac{1}{2\sigma^2} c^2$, which can be seen in Figures 10 and 12 (also subplots on the right).

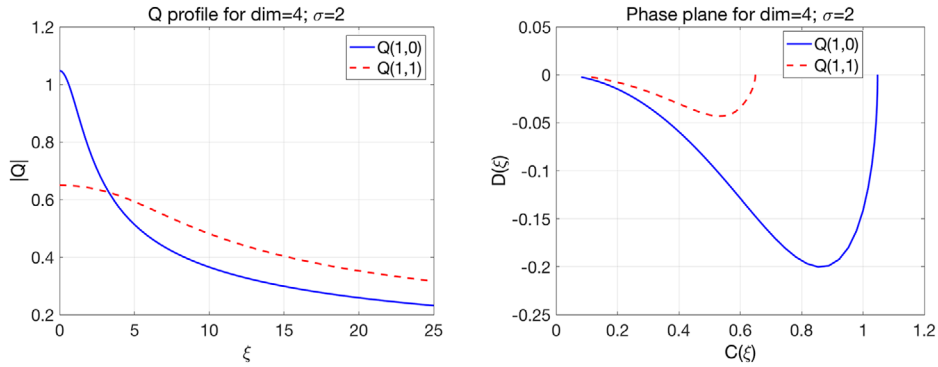

FIGURE 12 Q profile for $d = 4, \sigma = 2$. Left: the monotone solution $Q_{1,0}$ (blue) and the first bifurcation solution $Q_{1,1}$ (red). Right: the phase plane (C, D), here $D \sim -C^2$

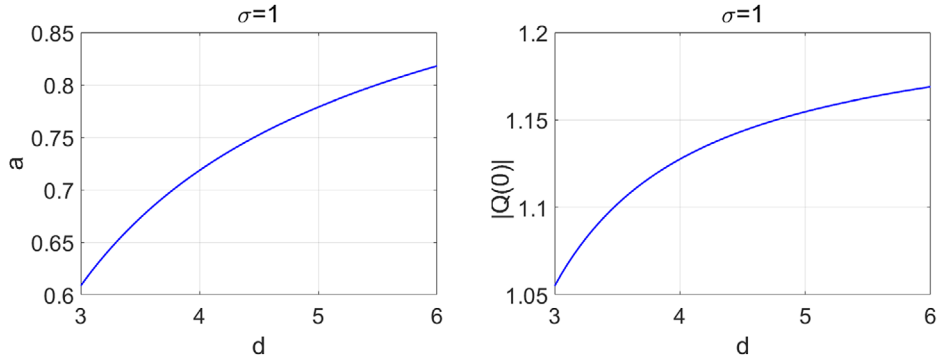

FIGURE 13 The change of a and $Q(0)$ with respect to the dimension d for $\sigma = 1$

If the solution Q oscillates fast at infinity, then its graph in the coordinates (C, D) will approach the origin in the oscillating manner, since

$$C \sim \frac{\alpha}{\xi^{1/\sigma}} \quad \text{and} \quad D \sim -\frac{\beta\, a}{\alpha}\, \frac{1}{\xi^{d-2/\sigma-1}}\, \sin\left(\frac{a\,\xi^2}{2} - \frac{2}{a}\log(\xi)\right).$$

Figures 9-12 (left subplots) are profiles of $|Q|$. We also show how the values of a and $Q(0)$ continuously change with respect to the dimension (taking d as a continuous parameter) in Figure 13 ($\sigma = 1$) and Figure 14 ($\sigma = 2$). Table 9 contains the values for a and $Q(0)$ that we obtain in our simulations.

TABLE 9 The values for a and $Q(0)$ for the monotone solution $Q_{1,0}$ and first bifurcation solution $Q_{1,1}$

d	σ	$Q(1,0)$		$Q(1,1)$	
		a	$Q(0)$	a	$Q(0)$
3	1	0.60868	1.05512	0.21180	0.35569
3	2	1.40186	0.99765	0.31725	0.60782
4	1	0.71853	1.12757	0.22045	0.41841
4	2	1.57426	1.04749	0.32613	0.62799

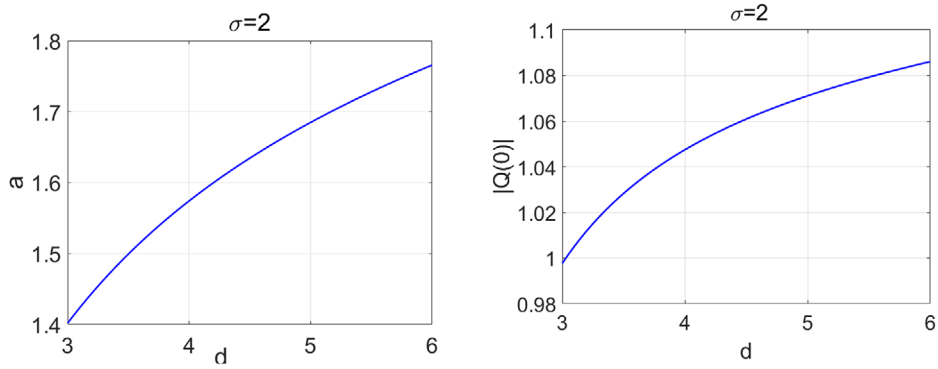

FIGURE 14 The change of a and $Q(0)$ with respect to the dimension d for $\sigma = 2$

5.3 | Direct simulation of the blow-up dynamics

We simulate the blow-up dynamics of the L^2-supercritical gHartree equation in the following cases:

- $3d$ $\sigma = 1$ ($s_c = \frac{1}{2}$ - energy-subcritical);
- $3d$ $\sigma = 2$ ($s_c = 1$ - energy-critical);
- $4d$ $\sigma = 1$ ($s_c = 1$ - energy critical) and
- $4d$ $\sigma = 2$ ($s_c = \frac{3}{2}$ - energy-supercritical).

We take the initial data $5e^{-r^2}$ for the nonlinearity $\sigma = 1$, and $2.5e^{-r^2}$ for the nonlinearity $\sigma = 2$. Such initial data lead to the negative energy for the case $d = 3$ and positive energy for $d = 4$.

The numerical results shown for the super-critical case are computed by the finite difference discretization described in Section 3. We terminate our simulation when $L(t) < 10^{-24}$, though for clarity most of the results are presented only up to $L(t) \sim 10^{-20}$.

For the L^2-supercritical case ($s_c > 0$), it is easy to follow the analysis for $a(\tau)$ in Ref. 50 (see also Ref. 19) to obtain the blow-up rate, as again, the nonlinear term plays no role in the asymptotic analysis. Thus, the blow-up rate is predicted to be

$$L_{\text{pred}}(t) \approx (2a(T-t))^{\frac{1}{2}}. \tag{103}$$

Note that if $Q(\xi)$ is the profile obtained when solving (16), and $\tilde{Q}(\eta)$ is another profile with $\|\tilde{Q}\|_{L^\infty} = |\upsilon_0(0)|$ (e.g., we know that $Q(0) \approx 1.05$ for $d = 3$ and $\sigma = 1$ from Table 9 but we set $\|\tilde{Q}\|_{L^\infty} = |\upsilon_0(0)| = 1$ in our numerical simulation of the blow-up dynamics), then from (11), we have a family of Q profiles

$$Q(\xi) = \left(\frac{Q(0)}{\tilde{Q}(0)}\right)\tilde{Q}\left(\xi\left(\frac{Q(0)}{\tilde{Q}(0)}\right)^{\sigma}\right). \tag{104}$$

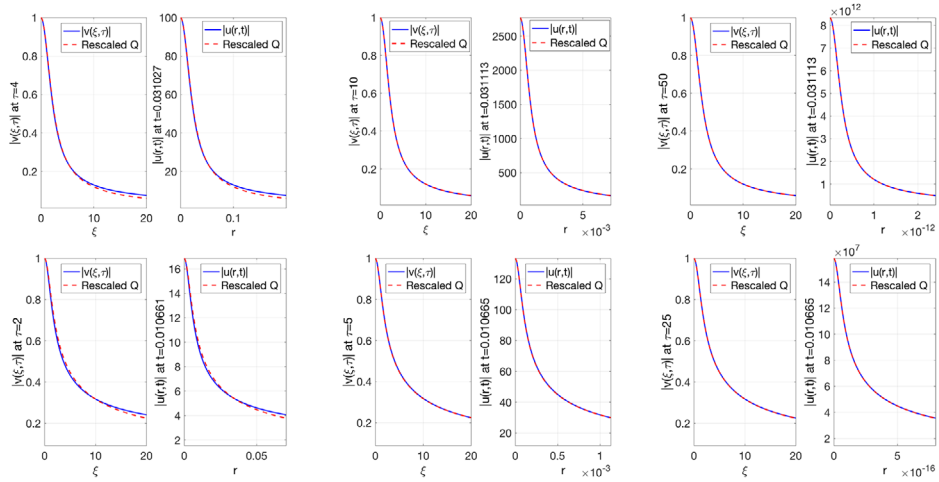

FIGURE 15 Blow-up profiles for the case $d = 3$: $\sigma = 1$ (top) and $\sigma = 2$ (bottom) at different times

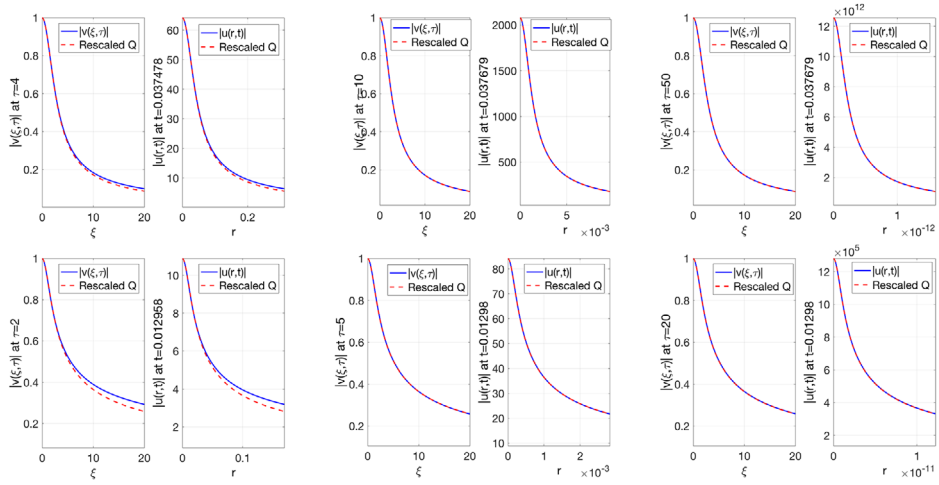

FIGURE 16 Blow-up profiles for the case $d = 4$: $\sigma = 1$ (top) and $\sigma = 2$ (bottom) at different times

Consequently, the corresponding rescaled $\tilde{a}$ satisfies

$$\tilde{a} = a\left[\frac{|\upsilon_0(0)|}{Q(0)}\right]^{2\sigma}. \tag{105}$$

For simplicity, we still use Q to represent the family of Q profiles, adding "up to scaling."

In Figures 15-18, we provide the following results from our simulations: blow-up profiles, blow-up rate $\ln(L)$ versus $\ln(T-t)$, the value of $a(\tau)$ depending on time τ, the distance between Q and υ in time τ, that is,

$$\|\upsilon(\tau) - Q\|_{L^\infty_\xi},$$

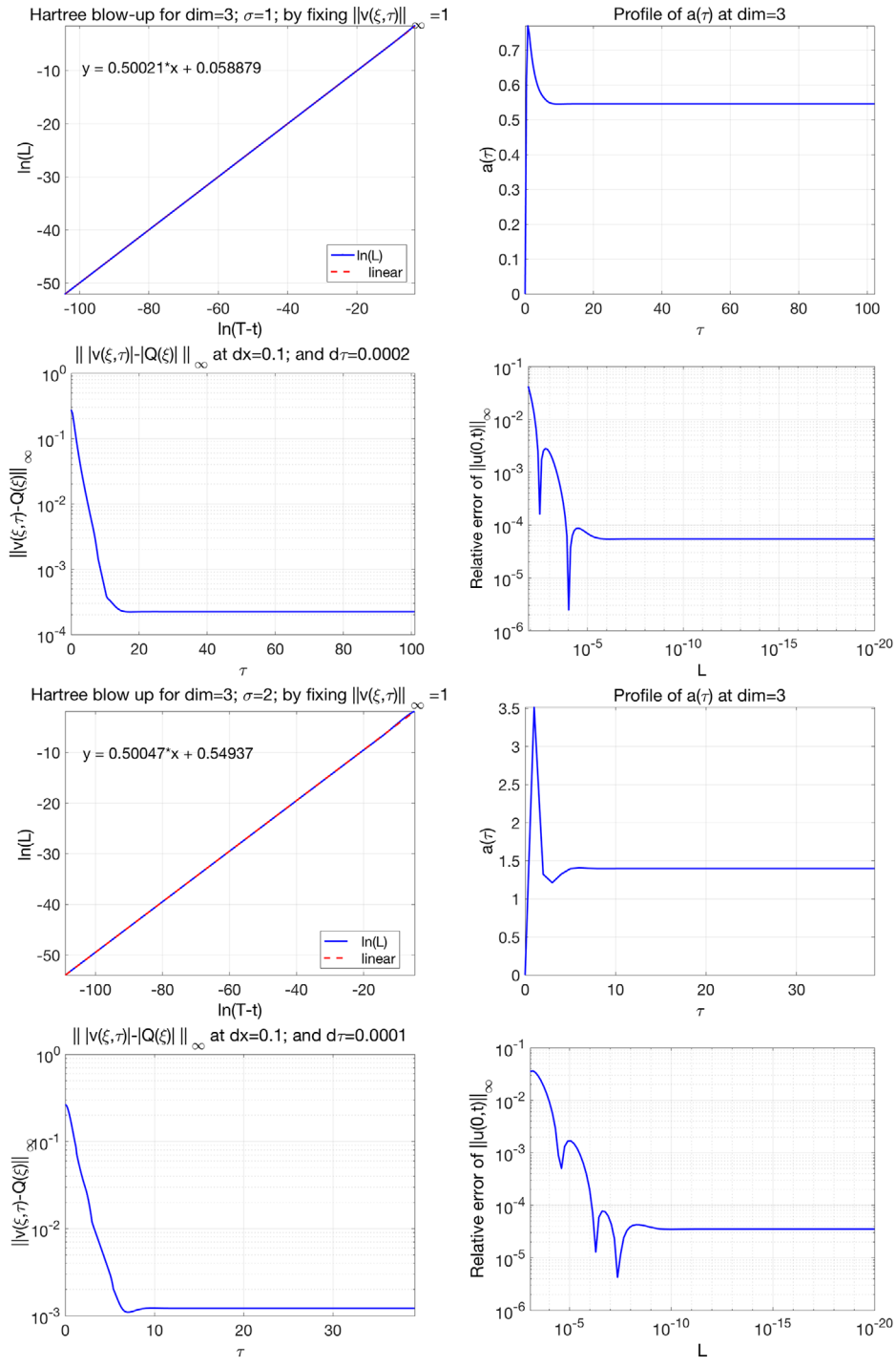

FIGURE 17 Blow-up data for the 3D cubic (top half) and 3D quintic(bottom half) cases: $\ln(T-t)$ versus $\ln(L)$ (upper left), the quantity $a(\tau)$ (upper right), the distance between Q and υ on time τ ($\|\upsilon(\tau)-Q\|_{L^\infty_\xi}$) (lower left), the relative error with respect to the predicted blow-up rate (lower right)

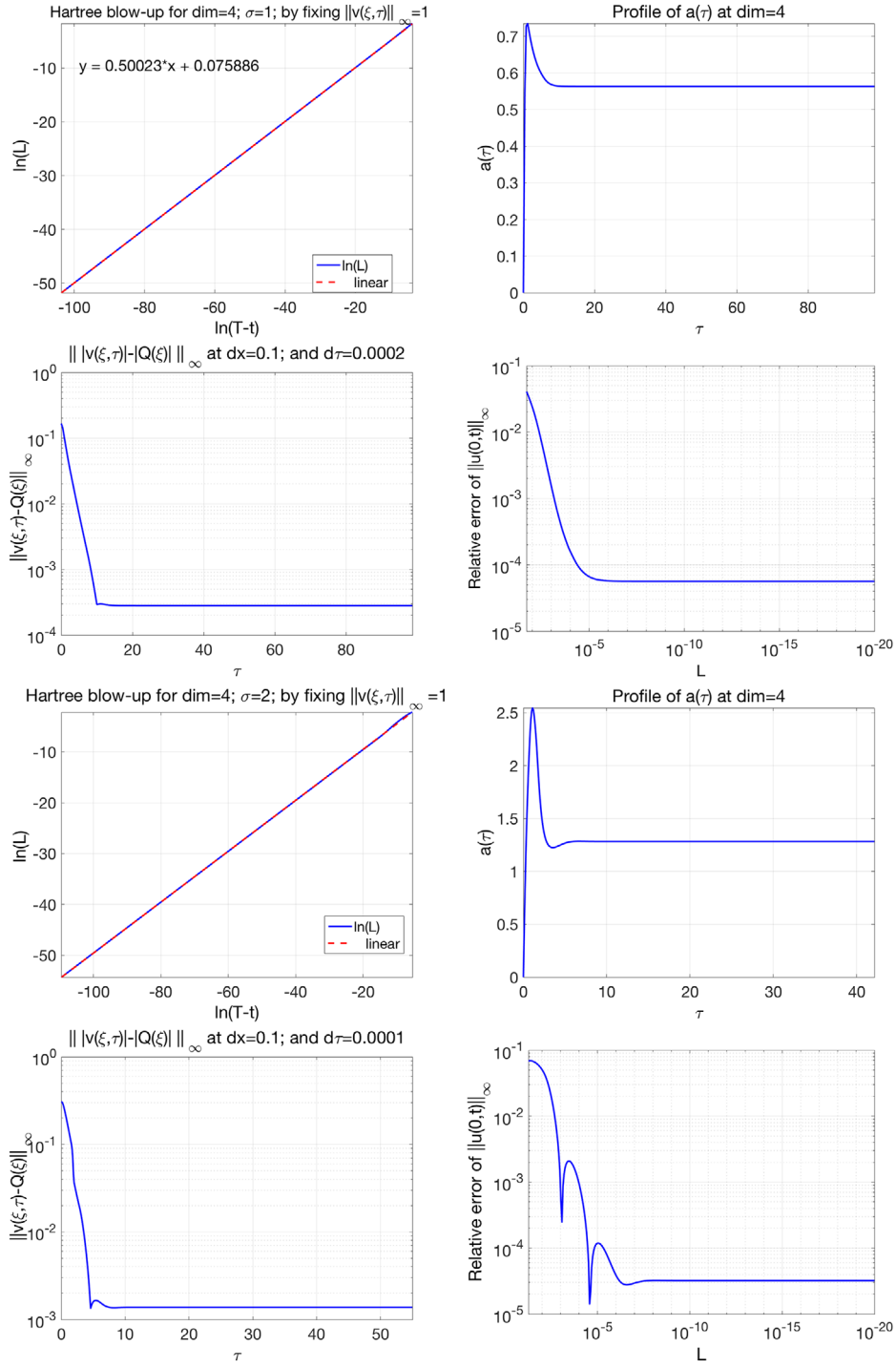

FIGURE 18 Blow-up data for the 4D cubic (top half) and 4D quintic (bottom half) case: $\ln(T-t)$ versus $\ln(L)$ (upper left), the quantity $a(\tau)$ (upper right), the distance between Q and υ on time τ ($\|\upsilon(\tau)-Q\|_{L^\infty_\xi}$) (lower left), the relative error with respect to the predicted blow-up rate (lower right)

and the relative error between the numerical results and the predicted rate, that is,

$$\mathcal{E}_{\text{rel}} = \left| \left(\frac{L(t)}{\sqrt{2\tilde{a}(T-t)}} \right)^{\frac{1}{\sigma}} - 1 \right|,$$

where $\tilde{a} = a(\tau_{\text{end}})$ is the value of a when we terminate our numerical simulation. In the numerical computation, the relative error $\mathcal{E}_{\text{rel}}$ is actually calculated by

$$\mathcal{E}_{\text{rel}} = \left| \exp\left(\frac{1}{2\sigma} (2\ln(L) - \ln(T-t) - \ln 2 - \ln \tilde{a}) \right) - 1 \right|$$

to make every term moderate (not to large or small), and thus, increase the accuracy.

In Figures 15 and 16, we show the convergence of the blow-up solution to the profile $Q_{1,0}$ (snapshots at different times), which we obtained in the previous subsection.

Figures 17 and 18 show:

1. the slope of $\ln(L)$ versus $\ln(T-t)$ is approximately $\frac{1}{2}$ (in all supercritical cases of gHartree equation that we considered);
2. the parameter $a(\tau)$ goes to a constant as $\tau \to \infty$;
3. the distance between the rescaled solution $v(\xi, \tau)$ and $Q(\xi)$ with respect to the time τ in the L^∞ norm, note that it is on the order 10^{-3} in all considered;
4. the relative error between the value $|u(0,t)|$ and the predicted blow-up rate $L_{\text{pred}}(t)$.

One can observe that our numerical simulations match the predicted $Q_{1,0}$ blow-up profile really well and the square root rate for $L(t)$ also has a nearly perfect fitting; computationally wise the matching is on the order of 10^{-3} and 10^{-5}, respectively. This confirms the Conjecture 2.

6 | CONCLUSIONS

This work is the *first* attempt to study stable blow-up solutions in the standard and generalized Hartree equations in both L^2-critical and L^2-supercritical cases, from asymptotical analysis approach and via numerical simulations.

We are able to obtain rates and blow-up profiles in the cases considered, and observe that the stable blow-up dynamics in the nonlocal gHartree equation is very similar to the NLS case. Such modification of nonlinearity does not affect the dynamics of the stable blow-up singularity formation. It would be interesting to investigate further this work rigorously as well as to understand whether there are modifications of nonlinearity or potentials (local or nonlocal, or a certain combination) such that the stable formation of singularity would change the dynamics in the singularity formation from the known NLS-type blow-up dynamics.

ACKNOWLEDGMENTS

KY and YZ would like to acknowledge Yongyong Cai, who hosted their visit to the Computational Science Research Center (CSRC) in Beijing during Summer 2017. KY would thank Anudeep Kumar Arora for his help on the background of the gHartree equation and further discussions and clarifications. SR was partially supported by the NSF CAREER grant DMS-1151618/1929029 and

DMS-1815873/1927258 as well as part of the KY's research and travel support to work on this project came from the above grants. SR would also like to thank the AROOO ("A Room of Ones's Own") initiative for focused research time for this project. YZ was partially supported by the Simons Foundation Grant No. 357963.

ORCID

Kai Yang https://orcid.org/0000-0002-2289-9403
Svetlana Roudenko https://orcid.org/0000-0002-7407-7639

REFERENCES

1. Lushnikov PM. Collapse and stable self-trapping for Bose-Einstein condensates with $1/r^b$-type attractive interatomic interaction potential. *Phys Rev A*. 2010;82:023615.
2. Lushnikov PM. Collapse of Bose-Einstein condensate with dipole-dipole interactions. *Phys Rev A*. 2002;66:051601.
3. Lenzmann E. Uniqueness of ground states for pseudorelativistic Hartree equations. *Anal PDE*. 2009;2(1):1-27.
4. Fröhlich J, Lenzmann E. Mean-field limit of quantum Bose gases and nonlinear Hartree equation. In *Séminaire: Équations aux Dérivées Partielles. 2003–2004*, Sémin. Équ. Dériv. Partielles, pages Exp. No. XIX, 26. École Polytech., Palaiseau, 2004.
5. Lieb EH. Existence and uniqueness of the minimizing solution of Choquard's nonlinear equation. *Stud Appl Math*. 1977;57(2):93-105.
6. Ginibre J, Velo G. On a class of nonlinear Schrödinger equations. I. The Cauchy problem, general case. *J. Funct Anal*. 1979;32(1):1-32.
7. Ginibre J, Velo G. Scattering theory in the energy space for a class of Hartree equations. In *Nonlinear Wave Equations* (Providence, RI, 1998, Contemp. Math., Vol. 263, pp. 29-60). American Mathematical Society, Providence, RI; 2000.
8. Lions P-L. The Choquard equation and related questions. *Nonlinear Anal*. 1980;4(6):1063-1072.
9. Lieb EH. The stability of matter and quantum electrodynamics. *Milan J Math*. 2003;71:199-217.
10. Fröhlich J, Jonsson BLG, Lenzmann E. Effective dynamics for boson stars. *Nonlinearity*. 2007;20(5):1031-1075.
11. Cazenave T. *Semilinear Schrödinger equations*. Providence, RI: American Mathematical Society; 2003.
12. Arora AK, Roudenko S. Global behavior of solutions to the focusing generalized Hartree equation. Forthcoming in Michigan Math. Journal, 2019, arXiv:1904.05339.
13. Arora AK, Roudenko S. On well-posedness and blow-up in the generalized Hartree equation. Preprint, 2019, arXiv:1910.01085.
14. Arora AK. *Singularities and Global Solutions in the Schrödinger-Hartree Equation*. [dissertation]. Miami, FL: Florida International University; 2020.
15. Krieger J, Lenzmann E, Raphaël P. On stability of pseudo-conformal blowup for L^2-critical Hartree NLS. *Ann Henri Poincaré*. 2009;10(6):1159-1205.
16. Xiang C-L. Uniqueness and nondegeneracy of ground states for Choquard equations in three dimensions. *Calc Var Partial Differential Equations*. 2016;55(6):134.
17. Moroz V, van Schaftingen J. Groundstates of nonlinear Choquard equations: existence, qualitative properties and decay asymptotics. *J. Funct. Anal*. 2013;265(2):153-184.
18. Moroz V, van Schaftingen J. A guide to the Choquard equation. *J Fixed Point Theory Appl*. 2017;19(1):773-813.
19. Fibich G. *The Nonlinear Schrödinger Equation*. Berlin: Springer; 2015.
20. Landman MJ, Papanicolaou GC, Sulem C, Sulem P-L. Rate of blowup for solutions of the nonlinear Schrödinger equation at critical dimension. *Phys Rev A*. 1988;38(8):3837-3843.
21. Sulem C, Sulem P-L. *The Nonlinear Schrödinger Equation*. New York, NY: Springer; 1999.
22. Yang K, Roudenko S, Zhao Y. Blow-up dynamics and spectral property in the L^2-critical nonlinear Schrödinger equation in high dimensions. *Nonlinearity*. 2018;31(9):4354-4392.
23. Yang K, Roudenko S, Zhao Y. Blow-up dynamics in the mass super-critical NLS equations. *Phys D*. 2019;396:47-69.

24. Fibich G, Merle F, Raphaël P. Proof of a spectral property related to the singularity formation for the L^2 critical nonlinear Schrödinger equation. *Phys D*. 2006;220(1):1-13.
25. Fibich G, Gavish N, Wang X-P. Singular ring solutions of critical and supercritical nonlinear Schrödinger equations. *Phys D*. 2007;231(1):55-86.
26. Fibich G, Gavish N, Wang X-P. New singular solutions of the nonlinear Schrödinger equation. *Phys D*. 2005;211(3-4):193-220.
27. Buslaev VS, Zakharov VE, Synakh V. Certain modes for wave collapse. *Sov J. Plasma Phys*. 1(Kraev. Zadachi Mat. Fiz. Smezh. Voprosy Teor. Funktsiĭ) 1975;24:335-338.
28. Goldman MV, Rypdal K, Hafizi B. Dimensionality and dissipation in Langmuir collapse. *Phys Fluids*. 1980;23(5):945-955.
29. Sulem P-L, Sulem C, Patera A. Numerical simulation of singular solutions to the two-dimensional cubic Schrödinger equation. *Comm Pure Appl Math*. 1984;37(6):755-778.
30. McLaughlin D, Papanicolaou G, Sulem C, Sulem P. Focusing singularity of the cubic Schrödinger equation. *Phys Rev A*. 1986;34:1200-1210.
31. Vlasov S, Piskunova L, Talanov V. Structure of the field near a singularity arising from self-focusing in a cubically nonlinear medium. *Sov Phys JETP*. 1978;48:808-812.
32. Wood D. The self-focusing singularity in the nonlinear Schrödinger equation. *Stud Appl Math*. 1984;71:103-115.
33. Rypdal K, Rasmussen JJ. Blow-up in nonlinear Schrödinger equations. II. Similarity structure of the blow-up singularity. *Phys Scripta*. 1986;33(6):498-504.
34. Fraĭman GM. Asymptotic stability of manifold of self-similar solutions in self-focusing. *Zh Èksper Teoret Fiz*. 1985;88(2):390-400.
35. Landman MJ, LeMesurier BJ, Papanicolaou GC, Sulem C, Sulem P-L. Singular solutions of the cubic Schrödinger equation. In: Balabane M, Lochak P, Sulem C. eds. *Integrable Systems and Applications*. Berlin: Springer; 1989:207-217.
36. Zakharov V, Kuznetsov E. Quasi-classical theory of three-dimensional wave collapse. *Zh Éksper Teoret Fiz*. 1986;91:1310-1324.
37. Dyachenko S, Newell AC, Pushkarev A, Zakharov VE. Optical turbulence: weak turbulence, condensates and collapsing filaments in the nonlinear Schrödinger equation. *Phys D*. 1992;57(1-2):96-160.
38. Akrivis GD, Dougalis VA, Karakashian OA, McKinney WR. Numerical approximation of blow-up of radially symmetric solutions of the nonlinear Schrödinger equation. *SIAM J Sci Comput*. 2003;25(1):186-212.
39. Lushnikov PM, Dyachenko SA, Vladimirova N. Beyond leading-order logarithmic scaling in the catastrophic self-focusing of a laser beam in kerr media. *Phys Rev A*. 2013;88:013845.
40. Dyachenko SA, Lushnikov PM, Vladimirova N. Logarithmic scaling of the collapse in the critical Keller-Segel equation. *Nonlinearity*. 2013;26(11):3011-3041.
41. Malkin V. On the analytical theory for stationary self-focusing of radiation. *Phys D*. 1993;64:251-266.
42. Fibich G, Papanicolaou G. A modulation method for self-focusing in the perturbed critical nonlinear Schrödinger equation. *Phys Lett A*. 1998;239(3):167-173.
43. Perelman G. On the blow up phenomenon for the critical nonlinear Schrödinger equation in 1D. In: Sigal IM, Sulem C, eds. *Nonlinear Dynamics and Renormalization Group*. Providence, RI: American Mathematical Society; 2001:147-164.
44. Merle F, Raphael P. The blow-up dynamic and upper bound on the blow-up rate for critical nonlinear Schrödinger equation. *Ann of Math. (2)*. 2005;161(1):157-222.
45. Merle F, Raphael P. Profiles and quantization of the blow up mass for critical nonlinear Schrödinger equation. *Comm Math Phys*. 2005;253(3):675-704.
46. Le Coz S, Martel Y, Raphaël P. Minimal mass blow up solutions for a double power nonlinear Schrödinger equation. *Rev Mat Iberoam*. 2016;32(3):795-833.
47. Martel Y, Raphaël P. Strongly interacting blow up bubbles for the mass critical nonlinear Schrödinger equation. *Ann Sci Éc Norm Supér. (4)*. 2018;51(3):701-737.
48. Budd CJ, Chen S, Russell RD. New self-similar solutions of the nonlinear Schrödinger equation with moving mesh computations. *J Comput Phys*. 1999;152(2):756-789.
49. Burton Ta. *Volterra Integral and Differential Equations*. 2nd ed. Amsterdam: Elsevier BV; 2005.
50. LeMesurier BJ, Papanicolaou GC, Sulem C, Sulem P-L. Local structure of the self-focusing singularity of the nonlinear Schrödinger equation. *Phys D*. 1988;32(2):210-226.

51. Shen J, Tang T, Wang L-L. *Spectral Methods: Algorithms, Analysis and Applications*. Heidelberg: Springer; 2011.
52. Trefethen LN. *Spectral Methods in MATLAB*. Philadelphia, PA: Society for Industrial and Applied Mathematics (SIAM); 2000.
53. Kopell N, Landman M. Spatial structure of the focusing singularity of the nonlinear Schrödinger equation: a geometrical analysis. *SIAM J Appl Math*. 1995;55(5):1297-1323.
54. Pelinovsky DE, Stepanyants YA. Convergence of Petviashvili's iteration method for numerical approximation of stationary solutions of nonlinear wave equations. *SIAM J Numer Anal*. 2004;42(3):1110-1127.

How to cite this article: Yang K, Roudenko S, Zhao Y. Stable blow-up dynamics in the L^2-critical and L^2-supercritical generalized Hartree equation. *Stud Appl Math*. 2020;1–49. https://doi.org/10.1111/sapm.12328

APPENDIX A

Here, we compute the ground state Q via the renormalization method from (Refs. 19, chapter 28; 54). We rewrite Equation (8) as

$$(-\Delta + 1)Q = \mathcal{N}(Q), \tag{A.1}$$

where $\mathcal{N}(Q) = ((-\Delta)^{-1}|Q|^p)|Q|^{p-2}Q$ is the nonlinear part. Multiplying the Q and integrating on both sides, we have

$$SL(Q) := \int_{\mathbb{R}^d} Q^2 = \int_{\mathbb{R}^d} Q(-\Delta + 1)^{-1}\mathcal{N}(Q) =: SR(Q). \tag{A.2}$$

To prevent the fixed point iteration from going to 0 or ∞, we multiply (7.2) by a constant c_i in each iteration, that is,

$$SL(c_i Q^{(i)}) = SR(c_i Q^{(i)}).$$

From above, we immediately have

$$c_i = \left(\frac{SR(Q^{(i)})}{SL(Q^{(i)})}\right)^{\frac{1}{2p-2}}. \tag{A.3}$$

Now, we can apply the fixed point iteration as follows

$$Q^{(i+1)} = (-\Delta_N + I_N)^{-1}\mathcal{N}(c_i Q^{(i)}) = \left(\frac{SR(Q^{(i)})}{SL(Q^{(i)})}\right)^{\frac{2p-1}{2p-2}}(-\Delta_N + I_N)^{-1}\mathcal{N}(Q^{(i)}) \tag{A.4}$$

until we reach the desired accuracy, say $\|Q^{(i+1)} - Q^{(i)}\|_\infty < 10^{-12}$ in our calculation. Here, $-\Delta_N$ is the discretized Laplacian operator of size $N + 1$ described in Section 2, and the I_N is the identity matrix of size $N + 1$.

Remark 8. We tried different nontrivial initial guesses for $Q^{(0)}$ (including different $Q^{(0)}(0)$), the algorithm always converges to the same profile $Q^{(\infty)}$. It is due to the convergence property of this algorithm, see Ref. 54. Although it does not answer the uniqueness of the profile question, numerically it suggests the uniqueness of the ground state.